# Integrated coastal vulnerability index for coastal flooding: A case study of the Croatian coast

**Marić, Ivan; Peer, Monika; Čipak, Anita; Kobaš, Kristian; Šiljeg, Ante; Krvavica, Nino**

Environmental and Sustainability Indicators 24 (2024) 100514

Contents lists available at ScienceDirect

Environmental and Sustainability Indicators

journal homepage: www.sciencedirect.com/journal/environmental-and-sustainability-indicators

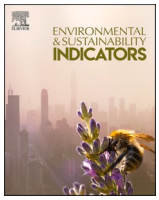

# Integrated coastal vulnerability index for coastal flooding: A case study of the Croatian coast

Ivan Marić [a,*], Monika Peer [b], Anita Čipak [b], Kristian Kobaš [b], Ante Šiljeg [a], Nino Krvavica [c]

[a] University of Zadar, Department of Geography, Center for Geospatial Technologies, Croatia
[b] University of Zadar, Department of Geography, Croatia
[c] University of Rijeka, Faculty of Civil Engineering, Croatia

ARTICLE INFO

*Keywords:*
Coastal vulnerability index
Coastal flooding
Integrated approach
GIS-MCDA

ABSTRACT

The combination of accelerated urbanization and tourism-related activities, along with frequent coastal flooding, has generated pressure on the coastline of the Republic of Croatia (RH). In this paper, an integrated coastal vulnerability model (ICVI) for coastal flooding was developed. The ICVI was generated using a GIS multicriteria approach and derived from two sub-indices: the physical vulnerability index ($CVI_N$) and the socio-economic vulnerability index ($CVI_S$). In total, 30 criteria were used in the derivation of the ICVI, with twelve contributing to $CVI_S$ and eighteen to $CVI_N$. The ICVI model is represented as a line divided into smaller segments, each segment indicating ICVI vulnerability levels ranging from 1 (*very low*) to 5 (*very high*). The accuracy of $CVI_N$ was evaluated using 159 geocoded coastal flood locations obtained from various websites and the official register of Hrvatske Vode flood events from 2008 to 2023. More than 80% of geocoded flood locations are situated in areas with very high (5) or high (4) $CVI_N$. Furthermore, out of 32 settlements with officially registered flood events, 90.6% of them are located in areas with *very high* or *high* ICVI. Since all data used in the ICVI derivation were acquired from open-source databases and a user-friendly GIS-MCDA toolbox was utilized, this paper presents a cost-effective approach to modeling integrated coastal vulnerability. This model can guide decision-makers and provide them with new insights for implementing an effective integrated coastal zone management strategy.

## 1. Introduction and background

Coastal zones are highly dynamic, oscillating environments endangered by anthropogenic pressures and naturally related processes (Domazetović et al., 2021). Different approaches are used in delineating coastal areas (Batista, 2018; Liu et al., 2015; Ramnalis et al., 2023). The most straightforward approach is based on the elevation where the low-elevation coastal zone (LECZ) is used in defining *contiguous and hydrologically connected areas of land along the coast and below 10 m* (Liu et al., 2015). Also, the administrative approach is often applied (Ramnalis et al., 2023; Batista, 2018). LECZ is considered extremely vulnerable to different hazards due to the high concentration of population and economy-related infrastructure and activities (Koboević et al., 2012). The importance of adequate management of coastal zones is often emphasized (Portman et al., 2012).

The greatest hazard expected to threaten LECZ will be sea level rise (SLR) (Gornitz, 1991; Karymbalis et al., 2012; Karymbalis et al., 2014; Bilskie et al., 2014; Horton et al., 2020; Ružić et al., 2019; El-Shahat et al., 2021; Griggs and Reguero, 2021; Baldoni et al., 2024). Depending on the regional level the SLR can deviate significantly from the globally averaged rate (global mean sea level - GMSL). *Intergovernmental Panel on Climate Change* (IPCC) stated that GMSL increased by 0.20 m from 1901 to 2018. The average rate of SLR was 1.3 mm/year between 1901 and 1971, increasing to 1.9 mm/year between 1971 and 2006 and further increasing to 3.7 mm/year between 2006 and 2018. In the IPCC's newest report, this is classified as *high confidence* (IPCC et al., 2023). According to the IPCC's mildest scenario, the global SLR is expected to be 0.29–0.59 m by 2100. In the worst scenario and other recent studies (Vitousek et al., 2017), an increase of 0.51–2 m is expected by 2100 (IPCC et al., 2019).

The risk increases when the population and economy are concentrated along coastal areas (McGranahan et al., 2007). An increase in coastal flooding frequency is recognized as a short-term effect of SLR (Bilskie et al., 2014; Vitousek et al., 2017). Coastal flooding occurs

* Corresponding author.
*E-mail addresses:* imaric1@unizd.hr (I. Marić), monikapeer888@gmail.com (M. Peer), anitacipak@gmail.com (A. Čipak), kiki.kristian.2906@gmail.com (K. Kobaš), asiljeg@unizd.hr (A. Šiljeg), nino.krvavica@uniri.hr (N. Krvavica).

https://doi.org/10.1016/j.indic.2024.100514
Received 31 May 2024; Received in revised form 17 October 2024; Accepted 18 October 2024
Available online 19 October 2024

during exposure to combined oceanographic and hydrologic events, which can be storm surges, large waves, high tides, extreme precipitation, and mean sea-level anomalies (Vitousek et al., 2017; Wahl et al., 2015). Due to relative SLR, extreme sea level events that now have a 1-in-100-year probability are projected to occur at least once a year at more than half of all tide gauge locations by 2100, regardless of the scenario considered (*high confidence* in IPCC repoert from 2023). Additionally, other regional changes are projected, including an increase in the intensity of tropical cyclones and/or extratropical storms (*medium* confidence in IPCC report). The IPCC et al. (2023) reports that the observed adverse impacts of flood and storm-induced damages to cities in coastal areas, which are attributed to climate change, will continue to intensify globally (*high* to *very high* confidence).

The Mediterranean coast is a globally significant biodiversity hotspot, heavily influenced by a wide range of pressures (Šiljeg et al., 2020). It is considered a climate change hotspot, facing significant and increasing human impacts (Furlan et al., 2021). It contains many coastal plains that are expected to be particularly vulnerable to flooding, leading to significant property damage, habitat destruction and risks to human safety (Antonioli et al., 2017; Furlan et al., 2021). Data has shown an increase in absolute SLR of $2.6 \pm 0.2$ mm/yr on average across the Mediterranean for the 1993–2015 (Thiébault and Moatti, 2016). SLR is expected to increase with considerable variability along Mediterrane coasts (Loizidou et al., 2024).

Although less researched and less known, floods caused by extreme high sea levels also occur on the eastern, ie Croatian coast of the Adriatic Sea (Međugorac et al., 2015; UPRIMO, 2022). The Adriatic Sea high water levels usually occur during late autumn and winter (Međugorac et al., 2015). At the head of the basin, SLR due to the storm surges, in some cases, reaches >1 m. Although coastal settlements in the eastern Adriatic are considered less vulnerable, in recent times several extreme events are increasingly occurring (Međugorac et al., 2018). On the northern part of the Croatian coast, in the last 15 years, more frequent flooding has been observed (UPRIMO, 2022). If the sea level rises by 1 m, 54,910 people in 302 coastal settlements of Croatia will be flooded (Šimac et al., 2023).

Although the concept of vulnerability has been extensively used in hazard-related research, it lacks an acceptable definition (Cutter et al., 2009). In this paper, vulnerability is considered as *people's differential inability to deal with hazards, based on the position of groups and individuals within both the physical and social worlds* (Dow, 1992). The conceptualization of a vulnerability is based on the *hazards-of-place* (HOP) (Cutter, 1996) model, where socioeconomic and physical elements influence the vulnerability of a location. This index needs to integrate both natural and social component to effectively be used in coastal vulnerability assessment to specific hazard (UNISDR, 2004).

Coastal vulnerability index (CVI) is one of the most popular and straightforward methods (Gornitz, 1991. in Šimac et al., 2023). CVI is usually derived for hazards caused by climate change (Torresan et al., 2012). A single CVI can depict vulnerability to multiple climate change impacts (i.e. permanent sea level rise, storm surge, coastal flooding, coastal erosion) (Torresan et al. (2012) or single climate change impact, flooding (Balica et al., 2012), coastal erosion (Ariffin et al., 2023; Cissé et al., 2024) or SLR (Furlan et al., 2021). To implement the CVI in quantifying vulnerability to coastal flooding, the index should be expanded with additional criteria specifically related to factors such as high tides, rainfall, and others, since flooding can sometimes occur due to a simultaneous combination of several factors (compound flooding) (Wahl et al., 2015). Therefore, the derivation of a representative vulnerability index is extremely challenging (Giannakidou et al., 2020). A detailed methodological overview and history of coastal vulnerability index (CVI) development is given by Torresan et al. (2012), Furlan et al. (2021) and Šimac et al. (2023). In the derivation of CVI, most of the authors use between 6 and 19 variables (Ietto et al., 2018; Ružić et al., 2019; Šimac et al., 2023). Roukounis and Tsihrintzis (2022) and Šimac et al. (2023) point out a large number of vulnerability indices derived on the basis of physical-geographical (CVI,[1] CSI.[2]) and socio-economic parameters (SoVI,[3] SVI …) and those that unite them (CSoVI,[4] CVI,[5] MSCVI,[6] CCFVI,[7] CRI-MED,[8] ICVI,[9] CUIVI[10]). Since it is very straightforward ICVI is becoming increasingly popular in the management of coastal areas (Ng et al., 2019; Ramnalis et al., 2023; Yahia Meddah et al., 2023; Batzakis et al., 2024; Cissé et al., 2024).

The main objective of this paper is to develop the integrative ICVI for the coastline of the Republic of Croatia (RH). So far, CVIs or its variations have only been performed on regions in Croatia (Ružić et al., 2019; Šimac et al., 2023; Mićunović and Faivre, 2023). ICVI is derived as a combination of two sub-indices: the physical vulnerability index ($CVI_N$) and the socioeconomic vulnerability index ($CVI_S$) using GIS-MCDA (Yahia Meddah et al., 2023). The derived ICVI was evaluated using data from the cadastre of coastal floods reported in the Croatian media over the past 15 years and a register of flood events of *Hrvatske Vode* for the period from 2008 to 2023 (Vujičić, 2024).

What sets this study apart from others is the development of two sub-indices using a comprehensive set of 30 criteria that includes both physical and socio-economic vulnerability domains, primarily utilizing open-source data. Additionally, the methodological contribution of this study lies in the calculation of the mean ICVI for coastal settlements, achieved by segmenting the urban section of the coastline into smaller 25-m elements an calculating the average ICVI for specific settlements. In summary, while this study builds on established methodologies, its strength lies in the integration of multiple criteria and the novel application of segment-based ICVI calculation.

## 2. Study area

### 2.1. Physical-geographical characteristics of the republic of Croatia (RH) coastline

The study area of the research includes the entire coastline of the Republic of Croatia (RH). It covers the eastern coast of the Adriatic Sea from the Savudrija peninsula in the west to the Prevlaka peninsula in the southeast. The Adriatic Sea is the semi-enclosed northernmost part of the Mediterranean Sea approximately 800 km long and 200 km wide (Lipizer et al., 2014) with around 5% of its total area. The Strait of Otranto (72 km wide) separates it from the Ionian Sea.

The RH has 1244 islands, geographically divided into 78 islands, 525 islets, and 641 rocks and reefs. The total length of the Croatian sea coastline is 6176 km, of which the island's coastline is 4398 km (71% of the total sea coast) (Fig. 1) (Ministry of the SeaTransport and Infrastructure, 2011 in Rossi et al., 2020). The indentedness of the Croatian coast is eight times greater than the Italian coast (Viličić, 2014). The coastline of RH is predominantly karstic and steep with a very narrow coastal strip ranging from 1 to 5 km in width. It is often limited by mountain chains whose slopes frequently meet the coastline. Between the Zadar and Šibenik only two larger coastal plains exist, the western part of the Istrian coast and the northern Dalmatian coast (Barić et al., 2008). Along the coast, relatively small karstic rivers dominate. Most of the rivers have canyon-type estuaries.

The eastern Adriatic coast stretches in a NW-SE direction, and its current morphology is the result of its geological basement and climatic

[1] Coastal Vulnerability Index.
[2] Coastal Sensitvity Index.
[3] Social Vulnerability Index.
[4] Coastal Social Vulnerability Score.
[5] Composite Vulnerability Index.
[6] Multi-scale coastal Vulnerability Index.
[7] Coastal City Flood Vulnerability Index.
[8] Multi-scale Coastal Risk Index in the Mediterranean.
[9] Integrated Coastal Vulnerability Index.
[10] Coastal Urban Industrial Vulnerability Index.

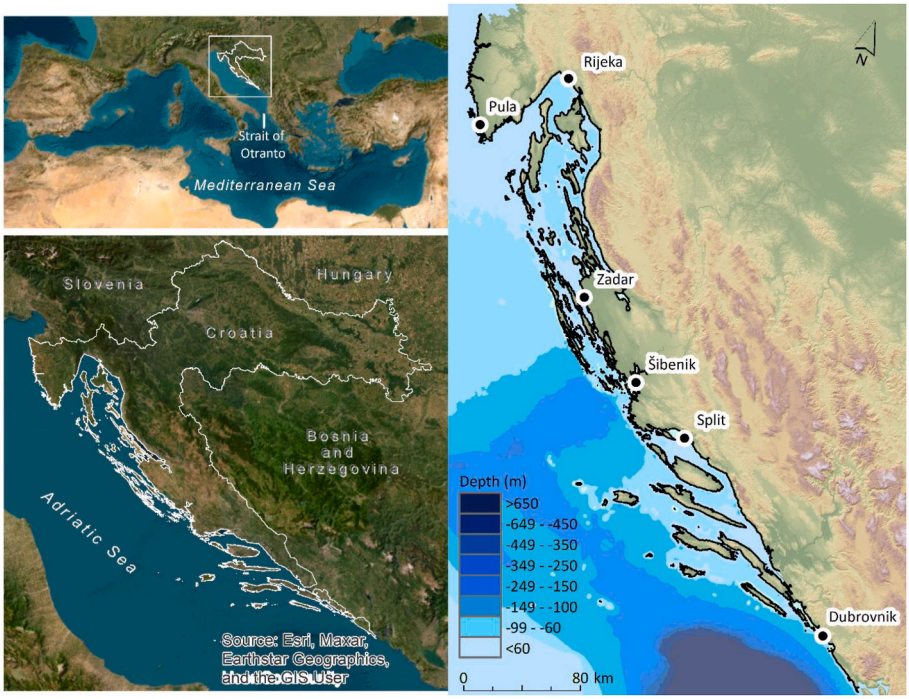


**Fig. 1.** Coastline of the Republic of Croatia.

changes that began in the upper Pleistocene. Its current shape is a result of the sudden rise in sea level (Flandrian transgression) which occurred during the early part of the Holocene epoch, beginning around 11,700 years ago and continuing until about 8000 to 6000 years ago (Stanley, 1995). The rise of the sea level submerged the former lowlands in the northwestern part of today's Adriatic Sea, as well as the lower areas along the coasts (Magaš, 2013). Therefore, the Adriatic Sea is classified as a relatively shallow and small sea. The total area of the Adriatic Sea is 138,595 km$^2$ (Magaš, 2013). The average depth is 252 m, and about 75% of the Adriatic is shallower than 200 m (Magaš, 2013). The geomorphological seabed of the Adriatic Sea consists of several parts: shallow northwestern part (depth up to 50 m), Jabučka basin (depth 245 m), Palagruža sill (130 m), and South Adriatic Bay (1330 m). As a result, it is often divided into the Northern (shallowest), Central and Southern (the deepest) Adriatic (Magaš, 2013; Viličić, 2014). The border between the northern and central Adriatic is the Jabučka basin. The southern and central Adriatic border on the Palagruža still (Viličić, 2014). Northern Adriatic is known for its significant river input and largest Mediterranean shelf area. The central Adriatic is characterized by an average depth of 140 m, while in the southern Adriatic, linked to the Ionian Sea through the Otranto Sill, there is an increase in depth and it contains the Adriatic's deepest point reaching 1200 m (Kraus et al., 2019).

The eastern Adriatic coast is characterized by a complex wave regime

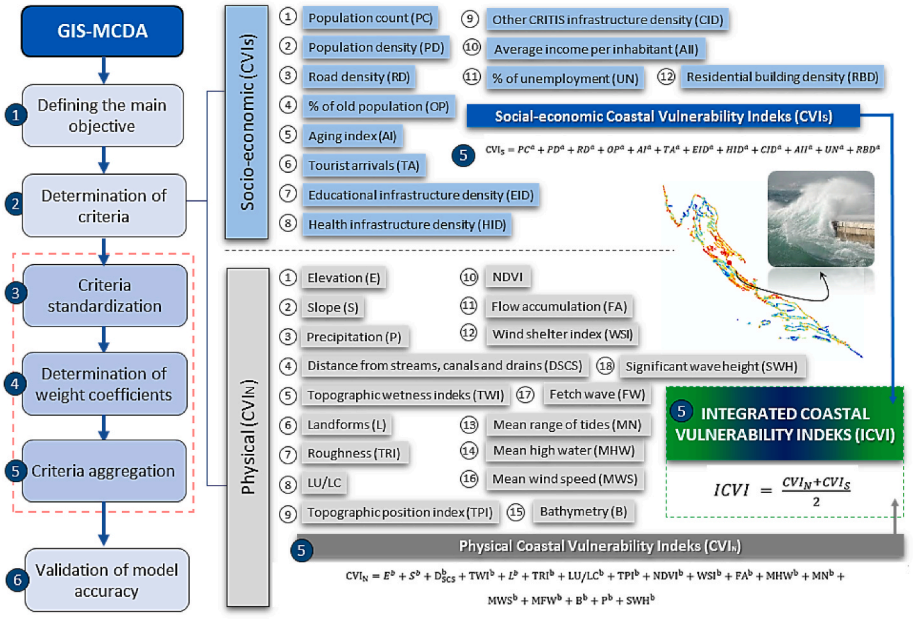


**Fig. 2.** GIS-MCDA methodological workflow.

**Table 1**
List of the criteria used in socio-economic vulnerability index ($CVI_S$) derivation.

| Sub-index | Criteria | Data Source | Literature (same or similar criteria) |
|---|---|---|---|
| Socioeconomic vulnerability ($CVI_S$) | Population count (PC) | World PoP, (2023a) | Mani Murali et al. (2013); Tragaki et al. (2018); Yahia Meddah et al. (2023); Satta et al. (2016) |
| | Population density (PD) | World PoP, (2023b) | Mavromatidi et al. (2018) |
| | Road density (RD) | Geofabrik | Mclaughlin and Cooper (2010); Gargiulo et al. (2020); Yahia Meddah et al. (2023) |
| | % of old population (OP) | DZS (2022) | Szlafsztein and Sterr (2007); Zanetti et al. (2016); Tragaki et al. (2018); Gargiulo et al. (2020), |
| | Ageing index (AI) | DZS (2022) | Mavromatidi et al. (2018) |
| | Tourist arrivals (TA) | DZS (2022) | Satta et al. (2016); Yahia Meddah et al. (2023) |
| | Educational infrastructure density (EID) | Ministry of Science and Education (2024) | Satta (2014); Debortoli et al. (2019); Hawchar et al. (2020) |
| | Health infrastructure density (HID) | Ministry of Health (2024); Geofabrik, HLJK (2024), Geofabrik | Satta (2014); Debortoli et al. (2019); Hawchar et al. (2020) |
| | Other critical infrastructure density (CID) | Geofabrik | Palmer et al. (2011); Johnston et al. (2014) |
| | Average income per inhabitant (AII) | Ministry of Regional Development and Funds of the EU (2024) | Mavromatidi et al. (2018); Rabby et al. (2019), |
| | % of non-employment (UN) | Ministry of Regional Development and Funds of the EU (2024) | Mavromatidi et al. (2018); Rabby et al. (2019) |
| | Residential buildings density (RBD) | Geofabrik | Palmer et al. (2011); Chao et al. (2021) |

influenced by complex morphology and the presence of many islands. The mean wave height (MWH) in this region varies depending on location and exposure to prevailing winds. Dominant winds in the Adriatic Sea that cause surface waves in winter are *bora* (N-NE to E-NE) and *sirocco* (E-SE to SS-E), while in the summer it is *maestral* (W-NW to NW) (Viličić, 2014; Katalinić et al., 2014). The *bora* is a cold and dry wind that mixes the water column, increasing evaporation, sea density, and heat loss (Dorman et al., 2006). It is strongest from December to March. The primary constraint on the development of *bora* wind waves is the relatively narrow fetch (Katalinić et al., 2014). The *sirocco* is a warm and humid wind, which is most intense in the channels between the coast and the islands that are open to the S-SE. The frequency of the *sirocco* is higher during the colder months and increases from the northern to the southern Adriatic (Viličić, 2014). Both the *bora* and *sirocco* can reach storm conditions and cause extreme wave events, whereas the *maestral* is a milder wind. During storm conditions, the *sirocco* can reach speeds of over 100 km/h, while maximum wave heights when *bora* is blowing can be between 6.2 and 7.2 m (Katalinić et al., 2014). Other winds that can generate surface waves in the Adriatic Sea include *ostro* (S), *libeccio* (W), *garbin* (SW), *ponent* (W), *tramontane* (N to NW), *levante* (E), and coastal circulation winds (Katalinić et al., 2014). Wind speeds and wave heights increase from the northern part of the Adriatic basin towards the south. Katalinić et al. (2014) found out that maximum mean annual significant wave height (SWH) for the Adriatic basin is 0.68 m, which is lower than the measurements reported by Queffeulou and Bentamy (2007), indicating a mean SWH of 0.85 m for period from 1992 to 2005. Also, 80% of SWH in the Adriatic Sea are below 1.10 m Katalinić et al. (2014). Katalinić and Parunov (2018) have calculated extreme wave heights in the Adriatic sea based on the Weibull distribution for different return periods. They concluded that extreme SWH values calculated for a 100-year return period are 8.48 m for the North, 7.10 m Central and 6.75 m for the South Adriatic respectively. Also, their analysis showed the mean yearly SWH has been increasing at a rate of around 0.05 m per decade.

The Adriatic Sea has a microtidal regime (Medvedev et al., 2020) where in some periods semidiurnal (SD) or diurnal (D) tides predominate. Diurnal tides are propagating from the Croatian to the Italian coast and the amplitudes are rising from the South to the North Adriatic. Although in most of the Mediterranean Sea, the mean tidal range does not exceed 20–30 cm (Lozano and Candela, 1995) in the Adriatic, higher values are recorded (Medvedev et al., 2020). Mean (D) tidal range along the eastern Adriatic coast, based on the long-term sea level measurements, is estimated to be 22 cm at Dubrovnik, 23 cm at Split, 25 cm at Zadar, 30 cm at Bakar and 47 cm at Rovinj. In the Gulf of Trieste, it can reach 1.2 m with the impact of the long-lasting *sirocco* and low air pressure (HHI, 2024). This can contribute to the formation of devastating floods in the northern Adriatic, in Venice (known as "acqua alta") (Bajo et al., 2019). Some parts of the Croatian coast are undergoing erosion and retreat, but of slightly lower intensity (Island of Susak, Vrgada and Nin) particularly where the natural sediment supply is low (Sokolić, 1994).

Sea-level measurements taken at four locations along the eastern Adriatic coast over the past 40 years show varying trends, with some areas experiencing an SLR between 0.53 and 0.96 mm/year, while others have seen a decrease between 0.50 and 0.82 mm/year, largely influenced by local tectonic activity (Barić et al., 2008).

### 2.2. Socio-economic characteristics of the republic of Croatia (RH) coastline

Based on the last official population census from 2021, 870,489 inhabitants, or ≈22.5% of the total Croatian population (3,871,833) live in settlements bordering the coast (DZS, 2022). The average population density of the settlements bordering the coast is 168 population/km,$^2$ while the average population density of settlements in the hinterland is 65.6 population/km.$^2$ The coastal zone of RH plays a significant role in the national economy (Ivandić and Šutalo, 2018) since tourism-related activities generate almost a fifth of the GDP of RH (Dukec et al., 2020). The primary economic activities in the coastal area revolve around the utilization of coastal resources, including tourism, fisheries and aquaculture, maritime transport, and shipbuilding (Barić et al., 2008). In 2023, a total of 19,492,931 tourist arrivals and 92,376,832 overnight stays were recorded in the RH. Of these, 16,934,300 arrivals (or 86.9%) and 87,351,814 overnight stays (or 94.6%) were recorded in the counties bordering the sea (DZS, 2024).

## 3. Material and methods

The GIS-MCDA is widely used in coastal vulnerability modeling (Mohamed, 2020; Barzehkar et al., 2021; Cissé et al., 2024). The workflow consisted of six steps (Fig. 2): (1) definition of the main objective, (2) determination of criteria; (3) criteria standardization; (4) determination of weight coefficients; (5) criteria aggregation and (6) accuracy assessment of the model (Domazetović et al., 2019).

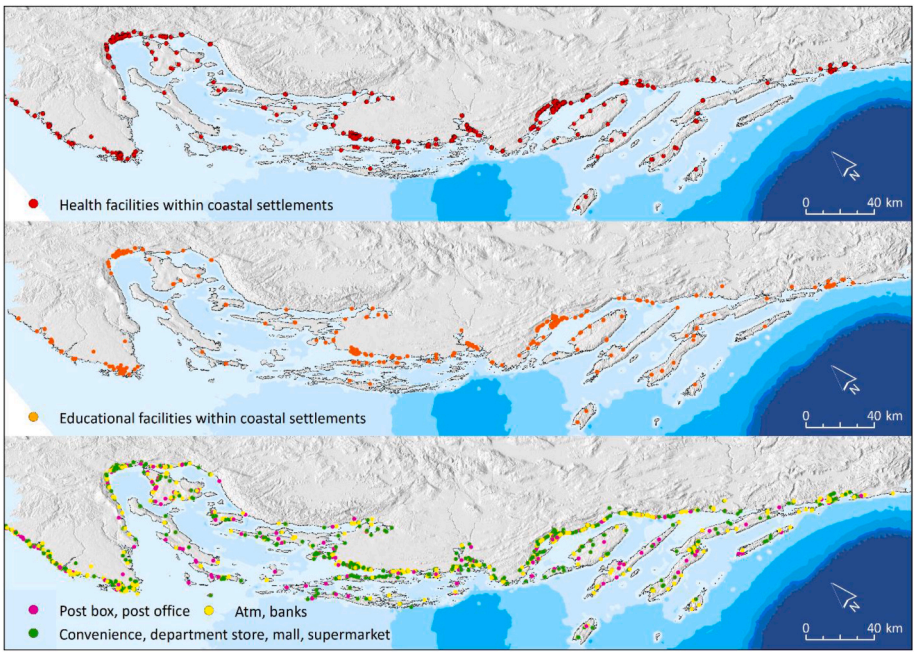


**Fig. 3.** Location of different critical infrastructure in coastal settlements.

### 3.1. Selection of vulnerability criteria

Vulnerability depends not only on the magnitude of the hazard but also on the socio-economic conditions of the population (Rabby et al., 2019).

#### 3.1.1. Socio-economic criteria

Twelve criteria were used in the derivation of $CVI_S$ (Table 1). Population count (PC) and density (PD) are recognized as important criteria due to the pressure exerted by the population and its activities on the coast. A larger population and higher population density negatively impact the coast, making it more vulnerable (Satta et al., 2016; Tragaki et al., 2018; Yahia Meddah et al., 2023).

The road network (RD) and residential building density (RBD) are considered a relevant socio-economic criterion. Coastal zones with a higher RD and RBD are more vulnerable (Gargiulo et al., 2020; Yahia Meddah et al., 2023). RD was calculated using the *Line Density* tool in ArcMap 10.8. RBD was calculated using the *Kernel Density*. The cell size of rasters was 25 m, while the search radius was set to 500 m. The share of the old population (OP) represents the percentage of the vulnerable group (+65 years) in the total population. The bigger the percentage, the vulnerability will be higher (Zanetti et al., 2016; Tragaki et al., 2018; Gargiulo et al., 2020). The ageing index (AI) refers to the number of the elderly population (+65) per 100 individuals younger than 14 years old in the population. The tourist arrivals (TA) have the same influence on vulnerability as the PC and PD. The bigger the number of tourists, the higher the vulnerability (Satta et al., 2016; Yahia Meddah et al., 2023). With the addition of this criteria we recognize the influence of the intensity of coastal tourism on coastal vulnerability, knowing previous findings that higher tourist numbers correlate with increased vulnerability (Satta et al., 2016; Yahia Meddah et al., 2023). This criteria is recognized as important since coastal tourism is a sector of central economic importance in Croatia. The important aspect is temporal dimension which could not be included. Coastal flooding mostly occurs outside the tourist high season, however, knowing the newest scenarios of climate change it is expected that the spring and autumn will be more suitable for tourism activities, increasing the overall risk of flooding (Toubes et al., 2017). Therefore, while it is recognized that seasonal population variations may indeed influence coastal conditions, our study focuses on assessing overall vulnerability patterns based on comprehensive demographic and socio-economic criteria throughout the year.

The density of critical infrastructures is important in modeling social aspects of vulnerability due to their importance in everyday life. Namely, climate change-induced elements are the main reasons for damage to coastal infrastructure (Bosello and De Cian, 2014). Therefore, a coastal zone is considered to be more vulnerable if the number of critical infrastructure near the coast is higher (Satta, 2014; Debortoli et al., 2019; Hawchar et al., 2020).

HID included geocoded locations of clinical hospitals, clinics, general hospitals, special hospitals, health centers, county institutes for emergency medicine, polyclinics, pharmacies, and public health service for general family medicine (Fig. 3). EID included geocoded locations of universities, secondary schools, primary schools and kindergartens. CID included banks, ATMs, technical inspection stations, post offices, malls, financial agencies, department stores, supermarkets and department stores (Fig. 3). The density of all infrastructure was derived using the Kernel Density tool in ArcMap 10.8.1. The cell size of the output raster was 25 m, while the search radius was set to 500 m. Average income per inhabitant (AII) is an economic indicator of wealth. Even if the magnitude of damage from specific hazards caught up the rich more in absolute terms, the poor population will still suffer greater relative damage due to their inability to cope with it (Felsenstein and Lichter, 2014). Therefore, the rate of unemployment (UN) is also used. It is considered that an area with a higher UN is generally more vulnerable to specific hazards (Mavromatidi et al., 2018).

#### 3.1.2. Physical-geographical criteria

Eighteen criteria were used in the derivation of $CVI_N$ (Table 2). The input model for deriving the morphometric parameters in $CVI_N$ was EUDEM. Areas with lower elevation and gentle slopes are more vulnerable to coastal flooding and more exposed to the influence of the sea (Gargiulo et al., 2020; Zampazas et al., 2022).

Areas closer to streams, canals, and drains (DSCS) have higher volumes of runoff during heavy rainfall events. This can contribute to flooding, especially if the drainage systems are ineffective. The

**Table 2**
List of the criteria used in physical-geographical vulnerability index ($CVI_S$) derivation.

| Sub-index | Criteria | Data Source | Literature (same or similar criteria) |
|---|---|---|---|
| Physical - geographical vulnerability ($CVI_N$) | Elevation (E) | EUDEM | Parthasarathy and Natesan (2015); Tragaki et al. (2018); Gargiulo et al. (2020); Zampazas et al. (2022); Šimac et al. (2023) |
| | Slope (S) | EUDEM | Parthasarathy and Natesan (2015); Tragaki et al. (2018); Gargiulo et al. (2020); Zampazas et al. (2022); Šimac et al. (2023) |
| | Distance from streams, canal and drains (DSCS) | Geofabrik | Bhattachan et al. (2018) |
| | Topographic wetness index (TWI) | EUDEM | Fitra et al. (2024) |
| | Landforms (L) | EUDEM | Mahapatra et al. (2015); Šimac et al. (2023) |
| | Topographic Roughness Index (TRI) | EUDEM | Osorio-Cano et al. (2019) |
| | LandUse/LandCover (LU/LC) | Corine Land Cover 2018 | Satta et al. (2016); Calil et al. (2017); Yahia Meddah et al. (2023) |
| | Topographic Position index (TPI) | EUDEM | Berman and Kuleshov (2023) |
| | Normalized difference vegetation index (NDVI) | Sentinel2 | Tibbetts and van Proosdij (2013); Pantusa et al. (2018) |
| | Wind Shelter Index (WSI) | EUDEM | – |
| | Flow Accumulation (FA) | EUDEM | Berman and Kuleshov (2023) |
| | Mean High Water (MHW) | ASTERION | Idier et al. (2019) |
| | Mean Range of Tides (MN) | ASTERION | Tano et al. (2016); Pantusa et al. (2018); Anfuso et al. (2021); Zampazas et al. (2022) |
| | Mean Wind Speed (MWS) | Global Wind Atlas | Zhang et al. (2021) |
| | Mean Fetch Wave (MFW) | Waves (2012) | Muler and Bonetti (2014) |
| | Bathymetry (B) | GEBCO | Parthasarathy and Natesan (2015) |
| | Precipitation (P) | WorldClim | Burkett and Davidson (2012); Ribas et al. (2020) |
| | Significant Wave Height (SWH) | Copernicus Marine Surface | Kumar et al. (2010); Tano et al. (2016); Pramanik et al. (2016); Anfuso et al. (2021) |

topographic wetness index (TWI) is a parameter that characterizes the potential for water accumulation and soil saturation. Higher values of TWI indicate low-lying areas prone to water accumulation. It may indicate depressions or valleys where water accumulates during flood. TWI was derived using the *Topographic Convergence Index (TWI)* tool from the *Topography Tools 10_3* toolbox. Landforms (L) provide information about type of the terrain topography. The criteria was derived using the *Landform Classification (Jenness)* tool from *Topography Tools 10_3* toolbox. Low-lying areas, such as valleys, or coastal plains are more prone to flooding. Terrain roughness index (TRI) affects the resistance of the land to the water flow. Higher R implies greater resistance. Criteria was derived using the *Roughness* tool in *Geomorphometry and Gradient Metrics (version 2.0)* toolbox. LU/LC cirteria was acquired from *CORINE Land Cover* website (Copernicus, 2024). Classes like *residential zones*, *commercial areas* and *industrial sites* have higher vulnerability to coastal flooding, while classes like *bare karst* and *sparsely vegetated* areas have lower vulnerability. The topographic position index (TPI) was derived in SAGA GIS 9.3.1. The TPI helps identify low-lying areas by analyzing the elevation of a pixel to its surroundings. Negative TPI values indicate depressions or valleys which are more susceptible to flooding. The NDVI measures the presence and greenness of vegetation, which can be useful for dispersing wave energy and reducing erosion in case of extreme events (Pantusa et al., 2018). The NDVI was derived from *Sentinel2a* imagery acquired from *Sentinel Hub.* The higher the NDVI value, the lower the vulnerability to coastal flooding is (Pantusa et al., 2018). The Wind Shelter Index (WSI) was calculated in SAGA GIS 9.3.1 for four wind directions that generate the largest waves along the Croatian coast. These include the *bora* (45°NE), the southeasterly *sirocco* (135°SE), the southerly *ostro* (180°S), and the southwesterly *libeccio* (225°SW). Mean WSI is then calculated as the mean value of these four WSI models. Therefore, the mean WSI was calculated to assess vulnerability of coastal areas based on their exposure to these predominant wind directions that cause the largest waves on the eastern Adriatic coast. In deriving the WSI, we considered not just wind directionality but also the alignment between wind vectors and coastline exposure, which amplifies vulnerability when these are aligned with the fetch. Flow Accumulation (FA) was derived in SAGA GIS 9.3.1 (*top-down*). It provides information about drainage patterns and potential flood pathways. Higher values of FA are more susceptible to flooding. Mean high water (MHW) represents the average height of the high tide over one-year period (2023) while mean range of tides (MN) represents the difference in height between mean high water and mean low water. Data of MHW and MN for marigraphic stations in the Adriatic Sea were acquired from the ASTERION website for 2023. Higher MHW and MN values indicate a greater risk of flooding during high tide (Pantusa et al., 2018; Zampazas et al., 2022). MHW and MN models were produced using *Create Thiessen Polygons* (Tragaki et al., 2018; Yahia Meddah et al., 2023). Mean wind speed (MWS) affects the coast due to the transport of particles and the generation of waves or storm surges. Higher MWS increases the vulnerability of the coastal area. The mean fetch wave (MFW) is important in modeling vulnerability to coastal flooding, particularly in the context of wave action and storm surges. Fetch refers to the distance over which wind blows across open water. Longer fetch distances allow waves to build up and gain more energy. Fetch wave model was derived using *Waves 2012* toolbox on the basis of DEM of the entire Adriatic Sea including the Strait of Otranto. The fetch model was generated for the same wind directions as in the WSI. The MFW is then calculated as the mean value of four FW models. Significant wave height (SWH) provides information about the average height of the highest one-third of waves. SWH was downloaded from Copernicus Marine Data Store for a period of time April 19, 2021 to April 2023. However, due to the highly indented Croatian coastline, regional reanalyses of SWH, such as MEDSEA, often underestimate values along the coast and around the islands (Bujak et al., 2023). On the other hand, data along the regular coastline are very accurate and reliable. Therefore, we recognize that regional reanalysis data, such as the MEDSEA dataset, may indeed underestimate SWH values along the highly indented Croatian coastline. However, SWH remains valuable in representing wave energy levels under average conditions, particularly along the smoother coastal segments where the data is reliable. Therefore, in addition to SWH, the analysis also includes mean wind speed (MWS) and mean fetch wave (MFW), both of which are key elements in determining the wave height. The bathymetry (B) data provides information about the underwater topography. This information is important in understanding wave dynamics. Shallower coastal areas are generally more vulnerable to coastal flooding because, as waves move into shallow water, they interact more with the seafloor. This interaction causes the waves to slow down, increase in height, and concentrate their energy, which can result in more powerful and destructive wave action

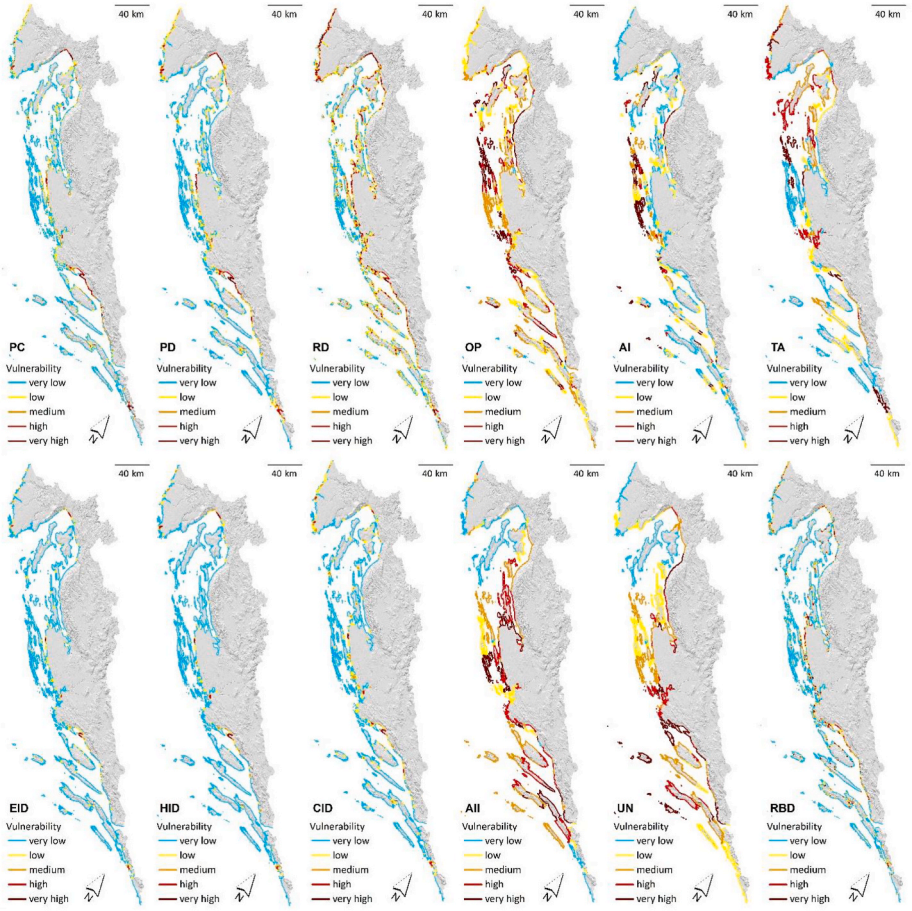


**Fig. 4.** Standardized criteria for socio-economic vulnerability index ($CVI_S$).

along the coast. In shallower waters, waves have more friction with the seafloor, causing them to change in height, wavelength, and energy. The precipitation (P) is a important factor in modeling vulnerability to coastal flooding. Higher the P increases vulnerability of the coastal area since it can contribute to increased runoff, leading to higher river discharge and potential flooding.

It was not possible to achieve consistency across all the data used for modeling the sub-indices ($CVI_S$ and $CVI_N$) in terms of spatial resolution and the time of data acquisition. This is very hard because of the (a) used data types which vary significantly (acquired using different sensors, acquisition techniques, various sources, and other factors); and (2) it was desirable to utilize open-source data, which limited our selection of data sources. However, it is important to note that such discrepancies in spatial and temporal resolution are characteristic of many studies on coastal vulnerability modeling. Despite these challenges, defined data was used to ensure the integration of all critical criteria necessary for a comprehensive assessment of coastal vulnerability, even though the spatial and temporal resolutions are not perfectly aligned.

### 3.2. Criteria standardization

To make different criteria comparable, they need to be reclassified on the same scale. Standardization was done using combination of *Jenks (natural breaks)* method and decision maker method (Marić et al., 2021; Cissé et al., 2024). The $CVI_S$ criteria were all standardized using *Jenks natural breaks* classification method on a scale from 1 to 5 which indicate the vulnerability level: *very low* (1), *low* (2), *moderate* (3), *high* (4), and *very high* (5) (Fig. 4). In standardization of criteria for physical vulnerability index ($CVI_N$) Jenks and decision maker method have been used (Fig. 5) (Table 3).

### 3.3. Determination of weight coefficients and criteria aggregation

In aggregating criteria different methods have been used (Šimac et al., 2023). In this paper, each sub-index ($CVI_N$ and $CVI_S$) was calculated separately and then the final ICVI model was derived from them. After the standardization of all criteria (1–5) weights must be assigned to each criteria based on their relative importance. Since the ICVI integrates both physical ($CVI_N$) and socio-economic criteria ($CVI_S$) in the absence of accurate data on the relative impact of the selected indicators the simple average method of aggregation was used. It provides equal weightage to all selected critera within defined sub-indices illustrating the interdependency and complexity of coastal vulnerability (Yahia Meddah et al., 2023; Attri et al., 2022). Therefore, for each criteria standardized in the $CVI_S$ sub-index weighting coefficient of $a = 0.0833$ was assigned, while for the $CVI_N$ weighting coefficient of $b = 0.0555$ was assigned. Each sub-index was aggregated using the tool *Weighted Sum* in ArcMap, which adds up the classified values (1–5) of each criteria (Eq. (1). and Eq. (2)). Namely, Gornitz et al. (1997) in Šimac et al. (2023) stated that addition shows lower sensitivity to misclassification errors and missing data.

$$CVI_S = PC^a + PD^a + RD^a + OP^a + AI^a + TA^a + EID^a + HID^a + CID^a + AII^a + UN^a + RBD^a \quad (1)$$

where $CVI_S$ is socio-economic vulnerability index, PC is standardized population count, PD is population density, RD is road density, OP is old population percentage, AI is ageing index, TS is tourist arrivals, EID is educational infrastructure density, HID is health infrastructure density, CID is other critical infrastructure density, AII is the average income per

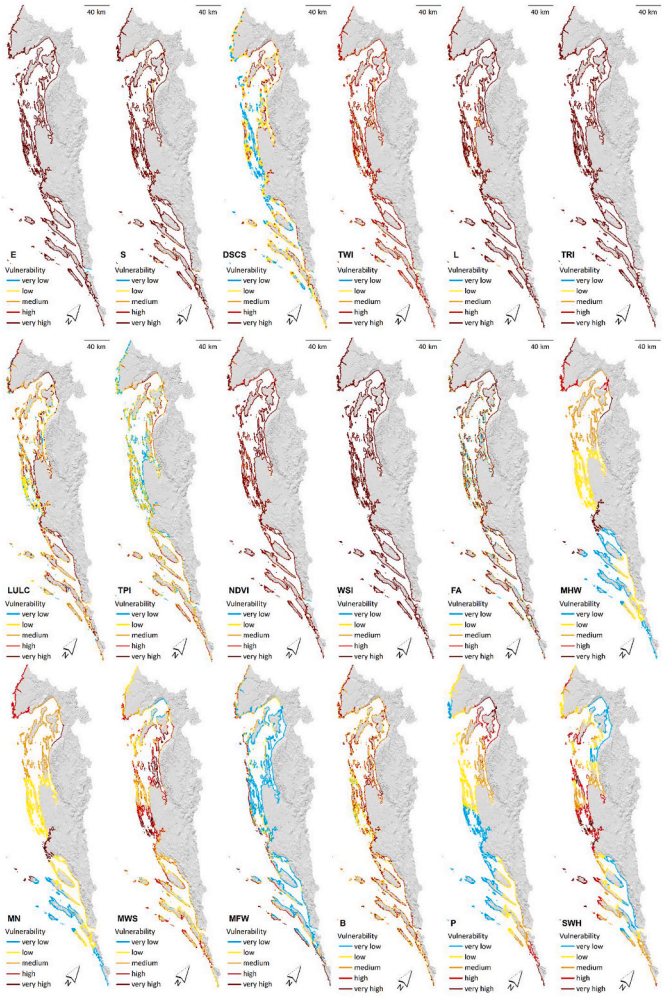


**Fig. 5.** Standardized criteria for physical vulnerability index ($CVI_N$).

inhabitant, UN is non-employment percentage, RBD is residential buildings density, $a$ is defined weight coefficient for CVIs criteria (0.0833).

$$CVI_N = E^b + S^b + D^b_{SCS} + TWI^b + L^b + TRI^b + LU/LC^b + TPI^b + NDVI^b + WSI^b + FA^b + MHW^b + MN^b + MWS^b + MFW^b + B^b + P^b + SWH^b \quad (2)$$

where $CVI_N$ is physical vulnerability index, E is standardized elevation, S is slope, DSCS is distance from streams, canals and drains, TWI is topographic wetness index, L is landforms, TRI is topographic roughness index, LU/LC is landuse/landcover, TPI is topographic position index, NDVI is normalized difference vegetation index, WSI is wind shelter index, FA is flow accumulation, MHW is mean high water, MN is mean range of tides, MWS is mean wind speed, MFW is mean fetch wave, B is bathymetry, P is precipitation, SWH is significant wave height, $b$ is defined weight coefficient for $CVI_N$ criteria (0.0555).

The final ICVI model was derived in *Raster Calculator* by summing the sub-indices ($CVI_N$ and CVIs) and dividing by the number of sub-indexes (Eq. (3)) (Szlafsztein and Sterr, 2007). Then, the vulnerability values were classified into five classes using the *Jenks* method. In future research, the adjustment of the weights based on expert judgment or sensitivity analysis will be.

$$ICVI = \frac{CVI_N + CVI_S}{2} \quad (3)$$

where ICVI is integrated coastal vulnerability model, $CVI_N$ is physical-geographical vulnerability index and $CVI_S$ is socio-economic vulnerability index.

### 3.4. Ranking of most vulnerable settlements

Determining the most vulnerables settlements to coastal flooding was based on the derived mean ICVI value and its urban section of the coastline. An urban section of the coastline refers to the part of a coastal settlement that directly borders or touches the sea and is characterized by human habitation and development. For example, Fig. 6 illustrates

**Table 3**
Standardized criteria for physical vulnerability index ($CVI_N$).

| Standardization method | Criteria | 1 (very low) | 2 (low) | 3 (medium) | 4 (high) | 5 (very high) |
|---|---|---|---|---|---|---|
| DECISION MAKER METHOD | (E) | >40 | 20–40 | 5–20 | 2–5 | 0–2 |
| | (S) | >32 | 12–32 | 5–12 | 2–5 | 0–2 |
| | (DSCS) | >5000 | 5000–2000 | 2000–500 | 500–100 | 0–100 |
| | (TRI) | >20 | 10–20 | 5–10 | 1–5 | 0–1 |
| | (L[a]) | 9, 10 | 7, 8 | 5, 6 | 3, 4 | 1, 2 |
| | (FA) | 0–1000 | 1000–5000 | 5000–10000 | 10000–20000 | >20000 |
| | (LU/LC) | 3.3.2, 4.2.3, 5.1.1, 5.1.2, 5.2.3 | 3.2.1, 3.2.2, 3.2.3, 3.3.3, 4.1.1, 4.2.1, 5.2.1 | 2.3.1, 3.1.1, 3.1.2, 3.13, 3.2.4, 3.3.1 4.2.2 | 1.3.1, 1.3.2, 1.3.3, 1.4.1, 2.1.1, 2.1.2, 2.2.1, 2.2.2, 2.2.3, 2.4.2, 2.4.3 | 1.1.1, 1.1.2, 1.2.1, 1.2.2, 1.2.3, 1.2.3, 1.4.2 |
| | (B) | < - 54 | −54–−15 | −15–−5 | −5–−2 | −2 - 0 |
| JENKS (NATURAL BREAKS) | (NDVI) | >0.22 | 0.22–0.15 | 0.15–0.1 | 0.1–0.05 | 0–0.05 |
| | (TWI) | 3.2–8.1 | 8.1–10.5 | 10.5–12.8 | 12.8–15.7 | 15.7–28.5 |
| | (TPI) | 25–−2.5 | −2.5–−6.3 | −6.3–−12.0 | −12.0–−24.0 | −24–−110.5 |
| | (WSI) | 0–41.2 | 41.2–54.7 | 54.7–66.7 | 66.7–81-4 | >81.4 |
| | (MHW) | 42.4–44.8 | 44.8–51.4 | 51.5–61.6 | 61.6–90.8 | >90.8 |
| | (MN) | 40.4–44.4 | 44.4–54.1 | 54.1–66-0 | 66.0–94.4 | >94.4 |
| | (PREC) | 35–63 | 63–75 | 75–87 | 87–100 | >100 |
| | (SWH) | 0–0.10 | 0.10–0.19 | 0.19–0.29 | 0.29–0.41 | >0.41 |
| | (MWS) | 1.5–3.7 | 3.7–4.9 | 4.9–5.9 | 5.9–7.1 | >7.1 |
| | (MFW) | 0–0.05 | 0.05–0.17 | 0.17–0.33 | 0.33–0.51 | >0.51 |

[a] 1 = canyons, deeply incised streams 2 = midslope drainages, shallow valleys 3 = upland drainages, headwaters 4 = u-shaped valleys 5 = plains 6 = open slopes 7 = upper slopes, mesas 8 = local ridges, hills in vallyes 9 = midslope ridges, small hills in plains, 10 = mountain tops, high ridges.

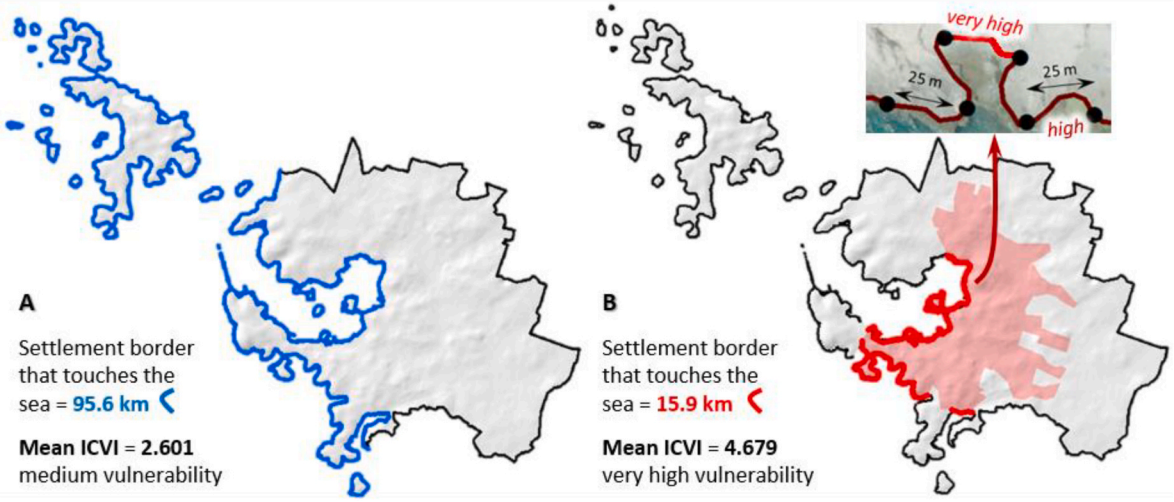


**Fig. 6.** Example showing the difference between deriving the mean ICVI for the city of Pula using (a) the entire coastline of the settlement versus (b) only its urbanized coastal section.

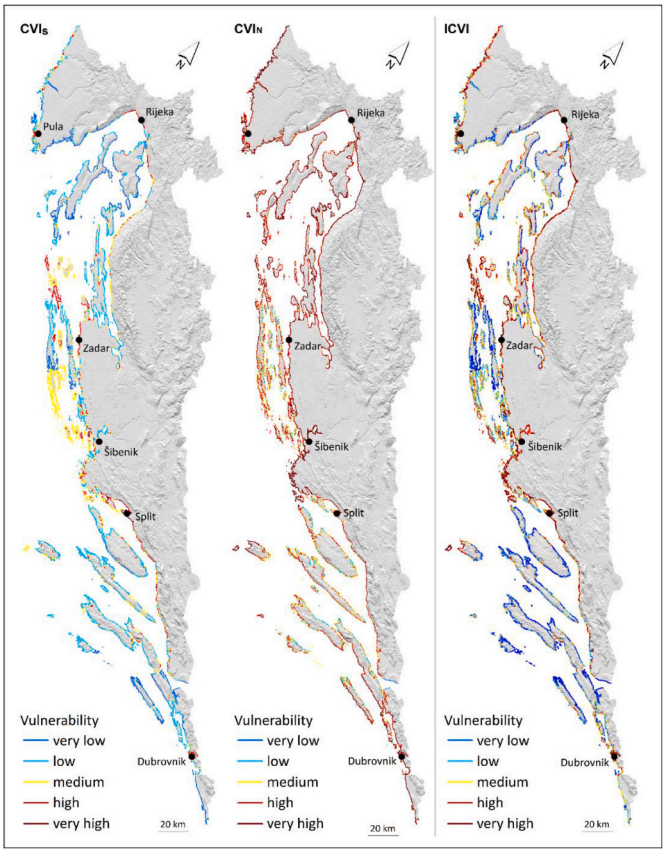


**Fig. 7.** Socio-economic ($CVI_S$), physical ($CVI_N$) and integrated coastal vulnerability index (ICVI).

the difference in the ICVI for the city of Pula when assessed under two scenarios: (a) based on the entire length of its coastline bordering the sea (94.6 km), and (b) based on only the portion of the coastline that is inhabited and developed (15.9 km). In scenario (a), the ICVI for Pula is 2.601 (class 3), indicating *medium* vulnerability. In contrast, in scenario (b), where only the developed coastal section is considered, the ICVI for Pula rises to 4.679 (class 5), indicating *very high* vulnerability.

The mean ICVI of specific settlement is calculated following this procedure. The urban section of the coastline (Fig. 6b) is divided into smaller segements (lines) with a distance of 25 m. A ICVI value from derived model was then joined to each line segement using the tool *Spatial Join* and function *Closest*. Thus, each settlements urban section of the coastline, had *n* smaller linear segments with a specific ICVI value (for example, Pula had around 330 elements). The mean ICVI of a specific settlement was then calculated using the tool *Dissolve* as the average ICVI value of the derived smaller segments. The clustering of line elements is made based on to the settlements ID code. In addition to the mean ICVI of a specific settlement, the length of the urban section of the coastline and the number of people living in settlement were added in attribute table.

**Table 4**
Lenght and share of vulnerability classes for coastline.

| Vulnerability Level (1–5) | CVIs | | $CVI_N$ | | ICVI | |
|---|---|---|---|---|---|---|
| | Lenght (km) | Share (%) | Lenght (km) | Share (%) | Lenght (km) | Share (%) |
| (1) very low | 1314 | 19.4 | 405 | 6.0 | 1764 | 25.98 |
| (2) low | 3058 | 45.0 | 1610 | 23.7 | 1501 | 22.11 |
| (3) medium | 1563 | 23.0 | 1515 | 22.3 | 1537 | 22.64 |
| (4) high | 716 | 10.5 | 1964 | 28.9 | 1120 | 16.49 |
| (5) very high | 139 | 2.0 | 1298 | 19.1 | 869 | 12.79 |

### 3.5. Validation of $CVI_N$ and ICVI accuracy

Accuracy assessment of the derived model was conducted using a cadastre of coastal floods reported in the Croatian online media over the past 15 years. Data acquisition was carried out based on the locations geocoded from online articles. Each location where the flood occurred had an ID associated with the date of the flood event and a link to the web article from which the information was acquired. Acquisition of location was done using *Google Earth Pro* and *ArcMap 10.8.1*. Therefore, the derived flood cadastre represented the reference ground data for the evaluation of the derived physical vulnerability index ($CVI_N$). For each geocoded location a vulnerability value, ranging from (1) *very low* to (5) *very high*, was added (using *Spatial Join—Closest*). The acquired flood events are compared with $CVI_N$ results considering that we could not acquire data about the infrastructural damages (which are more relevant to the $CVI_S$ results).

The accuracy assessment of the $CVI_N$ and ICVI models was also made on the basis of the *Register of Flood Events of Croatian Waters* for the period from 2008 to 2023. This dataset was acquired by Vujičić (2024).

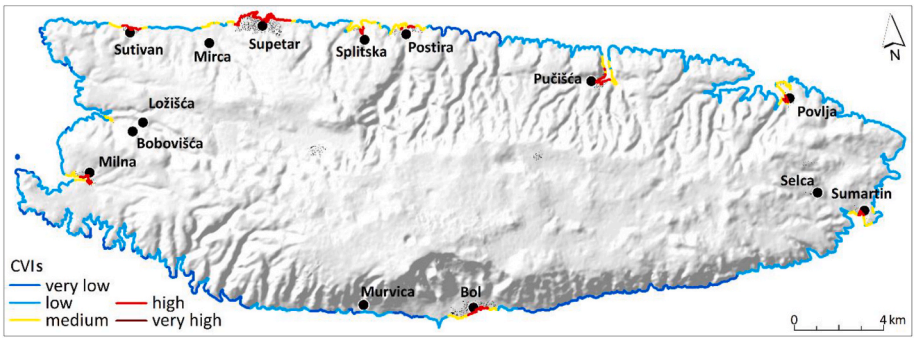


**Fig. 8.** CVIs for Brač island.

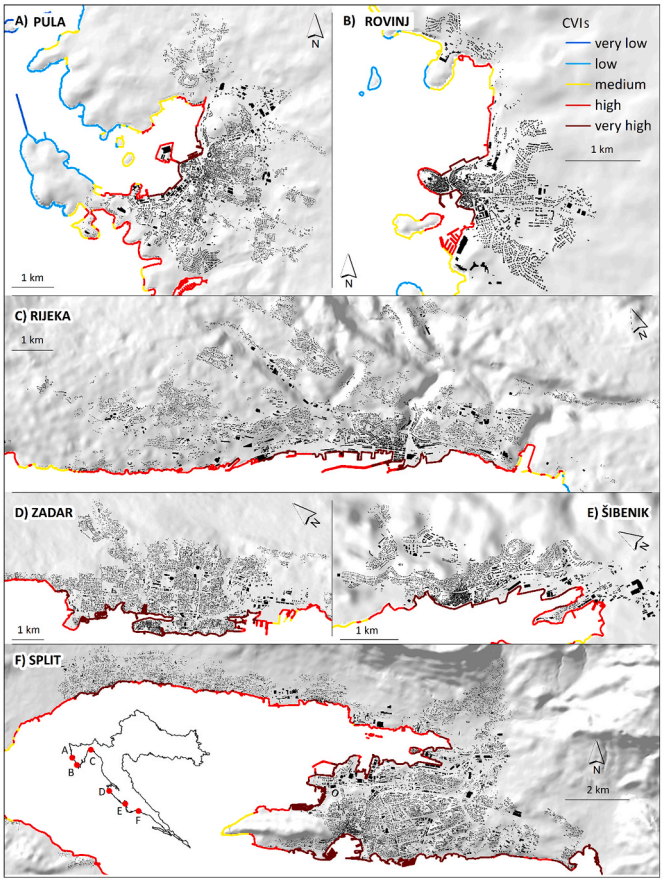


**Fig. 9.** Parts of coastline with higher CVIs.

## 4. Results and discussion

### 4.1. Derived vulnerability indices ($CVI_S$, $CVI_N$ and ICVI)

Given the wide range of global coastal conditions and varying research objectives, there is no one-size-fits-all Coastal Vulnerability Index (CVI). As a result, the indices used are always tailored to fit local conditions. In this study, we have performed the first national-scale assessment of physical ($CVI_N$), socio-economic ($CVI_S$) and final integrated coastal vulnerability (ICVI) model to coastal flooding (Fig. 7).

Table 4 shows lenght (km) and share of total coastline classified by vulnerability levels for $CVI_S$, $CVI_N$ and ICVI-. As expected, CVIs have a much smaller length or share of the coastline in the *very high* (5) and *high* (4) vulnerability classes. This is because in the $CVI_S$ modeling the selected criteria reflect the concentration of population and urban related elements and activities on the coast. The length and percentages of the classes in the $CVI_N$ model are similar in all vulnerability classes, with the exception of the *very low* class (1), which is several times smaller than the other classes and *very high* (5), which is in few percent smaller than *low, medium* and *high* classes.

The most vulnerable (5 - *very high*) parts of the coastline according to

**Table 5**
Larger coastal settlement ranked according to mean ICVI.

| Name | Mean_ICVI | Urban section of coastline (km) | Population (2021) |
|---|---|---|---|
| Zadar | 4.963 (very high) | 20.07 | 67309 |
| Šibenik | 4.912 (very high) | 8.19 | 31115 |
| Rovinj | 4.903 (very high) | 6.55 | 11629 |
| Kaštela | 4.757 (very high) | 15.17 | 37794 |
| Makarska | 4.696 (very high) | 4.80 | 12809 |
| Dubrovnik | 4.694 (very high) | 16.65 | 26922 |
| Pula | 4.678 (very high) | 16.59 | 52220 |
| Podstrana | 4.638 (very high) | 4.13 | 10403 |
| Split | 4.620 (very high) | 23.83 | 149830 |

**Table 6**
Smaller coastal settlement ranked according to mean ICVI.

| Name | MEAN_ICVI | Urban section of coastline (km) | Population (2021) |
|---|---|---|---|
| Senj | 5.000 (very high) | 4.41 | 4164 |
| Opatija | 4.928 (very high) | 7.10 | 5701 |
| Biograd na moru | 4.902 (very high) | 6.25 | 5601 |
| Umag | 4.901 (very high) | 6.04 | 6751 |
| Primošten | 4.898 (very high) | 4.77 | 1555 |
| Crikvenica | 4.846 (very high) | 4.73 | 6239 |
| Vodice | 4.839 (very high) | 5.65 | 6592 |
| Pag | 4.808 (very high) | 4.41 | 2322 |
| Brodarica | 4.720 (very high) | 5.55 | 2611 |
| Murter | 4.683 (very high) | 4.86 | 1920 |
| Poreč | 4.655 (very high) | 6.84 | 8841 |

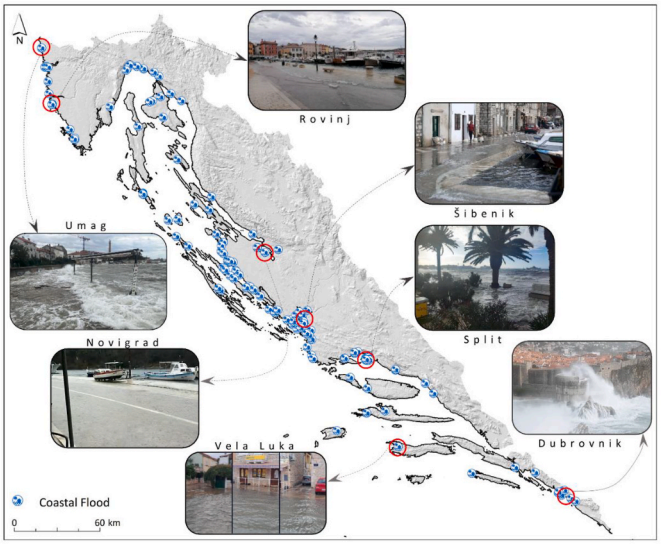


**Fig. 10.** Cadastre of coastal flood locations.

the $CVI_S$ are, as expected, parts of urban coastal areas of biggest cities of coast Split, Omiš, Makarska, Dubrovnik, Šibenik, Zadar, Trogir, Vodice, Šibenik, Rijeka, Rovinj, Dubrovnik, and Pula (Fig. 7). Then, the *high* (4) vulnerability class includes the coastal area of Poreč, Novigrad (Istria), most of the Opatija Riviera, Crikvenica, Novi Vinodolski, Vir, Biograd na Moru, Kaštela, Ploče, Umag, Primošten and larger settlements on the bigger islands (example Brač Island) (Fig. 8).

Namely, the intensity of vulnerability decreases with the reduction of human activities or urban content at the coastline. Thus, the areas of *highest* (5), *high* (4) and *medium* (3) vulnerability are associated with locations where there is pronounced touristic activity, road network density, critical infrastructure and population density (Fig. 9). Low values of CVIs are generally located in areas with little socioeconomic activity. *Very low* (1) vulnerability areas are found in inaccessible areas characterized by steep, difficult-to-access terrain. Considering that demographic criteria such as the share of the old population and the ageing index were also used in the process of performing CVIs, islands (Premuda, Molat) with a slightly less favourable demographic picture were recognized into categories of higher vulnerability.

All coastal settlements were then ranked according to mean ICVI. The most endangered larger settlements (n = 9) were singled out based on three criteria: (a) mean ICVI of urban section of coastline ≥4.5; (b) length of urban section of coastline >4 km and (c) population >10,000 (Table 5).

Also, the most endangered smaller settlements were singled out based on three criteria: (a) mean ICVI of urban section of the coastline ≥4.5; (b) length of urban section of coastline ≥4 km; (c) number of inhabitants ≤10000 and ≥300 (Table 6). These criteria are met by eleven settlements.

Despite the vulnerable physical-geographic characteristics of the croatian narrow coastal zone, urbanization, construction of apartments and tourist-related activities are still accelerating. Croatian newspaper articles frequently discuss the issue of floods affecting coastal cities (URL1). They mention flooded parts of Split (ICVI[11] is 4.62/*very high*), material damage in Istria, i.e. Pula (ICVI is 4.678/*very high*), Novigrad (ICVI - 4.511/*very high*) near Zadar and in Istria (ICVI - 4.975/*very high*), Kaštela (ICVI is 4.757/*very high*), Vodice (ICVI is 4.893 *very high*), Rab (ICVI is 4.857/*very high*), Rijeka (ICVI is 4.566/*very high*), Vela Luka (ICVI is 4.254/*high*), Hvar (ICVI is 3.917/*high*), Trogir (ICVI is 4.415/*high*), Šibenik (ICVI is 4.912/*very high*), Senj (ICVI is 5.000/*very high*) (URL1, URL4-6, URL8-14). In the future, the biggest flood events will be related to the northern Adriatic, where the tides and the *combination of southern-wester winds* are the most powerful. These will be Umag (ICVI is 4.901/*very high*), Novigrad (ICVI is 4.975/*very high*) in Istria, Poreč (ICVI - 4.654/*very high*), Rovinj (ICVI is 4.903/*very high*), Vrsar (ICVI is 3.941/*high*) which will be flooded in the future. Then there are towns that have a low waterfront, such as Cres (ICVI is - 4.167/*high*) (URL1-3, URL7). IPCC 6th Assessment Report Sea Level project that the city of Rovinj in 2100 will experience SLR of 0.64 m (SSP5-8.5).

### 4.2. Causes of coastal flooding

The most common cause of flooding in Croatian coastal settlements is the typical chain of mesoscale events over the Adriatic region, including a combination of strong to severe sirocco or scirocco, which carries warm Mediterranean air to the Adriatic and generates the cyclonic vortex (Brzović and Mahović, 1999), ultimately producing sea-level rise and high waves (Kolega, 2006). During the very strong wind, especially in the autumn and the first half of the winter, the sea level can rise over half a meter (Bernot, 1983). The waves, caused by the sirocco, can reach a height of a few meters. Forecasting is important because it induces high tides and flooding of the main low-lying coastal area of the northern Adriatic. Air pressure, cyclones, is the second atmospheric factor affecting sea level rise. During southeast winds and bad weather, air pressure can drop by more than 20 mb daily, which can cause the sea level to rise by 20 cm (Kolega, 2006). Therefore, extremely high levels of the Adriatic Sea are most often caused by storm surges caused by the passage of deep cyclones over the Adriatic area and the joint action of atmospheric air pressure and wind (Međugorac et al., 2018).

A factor that is not directly related to the cause of floods but makes this area predisposed to the occurrence of floods is the orientation and geomorphology of the Croatian coast (Dalmatian coasts) (Kelletat, 2019). The Croatian coast is primarily oriented in an NW-SE direction. It features numerous islands parallel to the coast and remnants of mountain ranges submerged by rising sea levels. The Croatian coast is mainly exposed the west, southwest, south and southeast. Namely, a large part of the coast, especially in the northern part near Istria, faces west, towards Italy across the Adriatic Sea. The central part of Dalmatia, where the coast has a slightly curved direction, is exposed to the southwest. The southern part of Dalmatia, including the areas around Dubrovnik, is exposed to the south, towards the open Adriatic. This type of orientation of the Croatian coast exposes it directly to wave action generated by predominant south-east (*sirocco*), south (*ostro*) south-west (*libeccio*) and west wind (*ponente*). This exposure increases vulnerability to coastal floods, driven by coastal orientation, wave dynamics and wind direction.

The predominant karst landscape of the Croatian coast, with its porous rock, can exacerbate the occurrence of coastal flooding. Heavy rainfall can lead to rapid runoff and swelling of rivers, while the same karst features limit the capacity for water absorption, thus increasing flood risks. Also, storm surges, particularly during severe weather conditions combined with rising sea levels due to climate change, can increase the potential for coastal flooding. The fact that coastal areas in Croatia are particularly popular tourist destinations, which are now experiencing significant development, does not make the situation any better.

Vujičić (2024) states that in the period from 2008 to 2023, the main cause of flooding was recognized in a sudden drop in air pressure on the day of the flood or a few days before, which was accompanied by a long-term rise in sea level. It is pointed that the occurrence and amount of precipitation in most cases do not coincide with flooding.

### 4.3. Cadastre of coastal floods

A total of 159 coastal flood locations were from acquired ranging

[11] Mean ICVI derived for urban section of coastline (km).


**Fig. 11.** Register of flood events (2008. - 2023.).
Source: modified according to the Vujičić, 2024.

**Table 7**
Comparison of settlements with registrated flood events and mean ICVI of settlements coasline

| Settlement | Number of floods | mean ICVI | mean $CVI_N$ | Settlement | Number of floods | mean ICVI | mean $CVI_N$ |
|---|---|---|---|---|---|---|---|
| Novigrad | 3 | 4.98/*very high* | 4.60/*very high* | Ist | 1 | 5.00/very high | 4.27/*high* |
| Antenal | 2 | 4.00/*high* | 5.00/*very high* | Biograd na Moru | 3 | 4.90/very high | 4.26/*high* |
| Tar - Vabriga | 3 | 3.80/*high* | 4.20/*high* | Vodice | 7 | 4.84/very high | 3.85/*high* |
| Poreč | 4 | 4.65/*very high* | 4.32/*high* | Zadar | 19 | 4.96/very high | 4.14/*high* |
| Vrsar | 2 | 3.94/*high* | 4.1/*high* | Šibenik | 7 | 4.91/very high | 4.60/*very high* |
| Rovinj | 7 | 4.90/*very high* | 4.60/*very high* | Rogoznica | 1 | 4.66/very high | 4.43/*high* |
| Pula | 5 | 4.68/*very high* | 3.89/*high* | Kaštela | 3 | 4.76/very high | 3.70/*high* |
| Opatija | 4 | 4.93/*very high* | 4.48/*high* | Trogir | 6 | 4.41/high | 2.84/*medium* |
| Volosko | 2 | 4.97/*very high* | 3.79/*high* | Split | 9 | 4.62/very high | 2.92/*medium* |
| Rijeka | 8 | 4.56/*very high* | 3.87/*high* | Omiš | 2 | 4.65/very high | 3.26/*medium* |
| Bakar | 8 | 3.79/*high* | 4.43/*high* | Hvar | 5 | 3.92/high | 3.01/*medium* |
| Crikvenica | 4 | 4.85/*very high* | 4.30/*high* | Stari Grad | 5 | 3.39/medium | 2.55/*medium* |
| Krk | 1 | 4.54/*very high* | 4.31/*high* | Jelsa | 1 | 2.09/low | 2.44/*low* |
| Rab | 1 | 4.86/*very high* | 4.36/*high* | Vela Luka | 7 | 4.25/high | 2.73/*medium* |
| Cres | 5 | 4.17/*high* | 4.33/*high* | Komolac | 1 | 4.63/very high | 4.38/*high* |
| Mali Lošinj | 4 | 2.86/*medium* | 3.14/*medium* | Dubrovnik | 6 | 4.69/very high | 4.00/*high* |

from Umag to Dubrovnik (Fig. 10). The flood locations were geocoded from the websites of local portals. Coastal flood locations included events that have occurred in the last 15 years.

A reclassified value ranging from 1 (*very low*) to 5 (*very high*) of $CVI_N$ was automatically added to each geocoded flood location (n = 159). This was done using the *Spatial Join* tool and Match option *Closest.* More than 80 % (n = 129) of flood locations are located on the coastline with *very high* (5) and *high* (4) physical vulnerability. Only 2.52 % (n = 4) of the flood locations is located on the coastline with *very low* (1) and *low* (5) physical vulnerability. These cases, in which a flood event was recorded, and the coastline has a *very low* or *low* ICVI, refer to flooding of boats along the coast itself, or a small flood of the waterfront. This results confirm the accuracy of the derived $CVI_N$.

A total of 146 coastal floods in 32 settlements were detected in the TU register of flood events of Croatian waters in the period from 2008 to 2023 (Fig. 11). Most were recorded in the northern Adriatic (63 flood events), 49 in the middle, and 34 in the southern (Vujičić, 2024, from Hrvatske vode, 2024).

For each of the 32 settlements in which the occurrence of flooding was registered, the mean $CVI_N$ and ICVI value of the urban section of the coastline was calculated. The derived mean $CVI_N$ and ICVI values are compared with the number of registered floods. For the mean ICVI, out of a total of 32 settlements, 29 of them (90.6%) belong to the *very high* (5) and *high* (4) vulnerability class. Two settlements (6.25%) are located in (3) medium vulnerability class and only one (3.125%) in *low* vulnerability class. None was recorded in the *very low* vulnerability class (Table 7). Regarding the mean CVIN, 24 settlements (75.0%) belong to the *very high* (5) and *high* (4) vulnerability class, seven (21.8%) to *medium* vulnerability class and one settlement in *low* vulnerability (3.125%). None was recorded in the *very low* vulnerability class. These

results confirm the accuracy of the derived ICVI (Table 7).

## 5. Conclusion

An integrated spatial vulnerability model (ICVI) to coastal flooding was derived for the coastal area of the Republic of Croatia (RH). ICVI is derived as a combination of the two sub-indices; physical vulnerability index ($CVI_N$) and the socioeconomic vulnerability index ($CVI_S$). In total, 30 criteria were used in the derivation of ICVI, twelve in the derivation of $CVI_S$ and eighteen in the derivation of $CVI_N$. The ICVI model is derived in the form of a line divided into smaller segments (distance of 25 m) where each segment has a classified value of integrated vulnerability ranging from 1 (very low) to 5 (very high). In total, around 2000 km, or 29.3% of RH coastline is classified in *very high* and *high* vulnerability class. The accuracy of $CVI_N$ was evaluated using 159 geocoded coastal flood locations acquired from various websites and the official register of *Hrvatske vode* which acquired flood events from 2008 to 2023. More than 80 % of geocoded flood locations are located on the coastline with *very high* (5) and *high* (4) of $CVI_N$. Furthermore, of 32 settlements with officially registered flood events, 90.6% belong to the *very high* and high *ICVI* vulnerability. In summary, Croatia's coast, with its unique geomorphological features and orientation, is vulnerable to coastal flooding due to its orientation, potential for storm surges, sea-level rise, and the effects of urbanization and tourism-related activities.

## CRediT authorship contribution statement

**Ivan Marić:** Writing – review & editing, Visualization, Software, Project administration, Methodology, Conceptualization. **Monika Peer:** Writing – original draft, Methodology, Investigation, Data curation. **Anita Čipak:** Methodology, Investigation, Data curation, Conceptualization. **Kristian Kobaš:** Investigation, Formal analysis, Conceptualization. **Ante Šiljeg:** Writing – review & editing, Visualization, Supervision. **Nino Krvavica:** Project administration, Funding acquisition.

## Declaration of competing interest

The authors declare the following financial interests/personal relationships which may be considered as potential competing interests: Ivan Maric reports article publishing charges was provided by Croatian Science Foundation. If there are other authors, they declare that they have no known competing financial interests or personal relationships that could have appeared to influence the work reported in this paper.

## Acknowledgments

This work has been supported and funded by the Croatian Science Foundation under the project IP-2022-10-7598.

## Data availability

Data will be made available on request.

## References

Anfuso, G., Postacchini, M., Di Luccio, D., Benassai, G., 2021. Coastal sensitivity/vulnerability characterization and adaptation strategies: a review. J. Mar. Sci. Eng. 9 (1), 72.

Antonioli, F., Anzidei, M., Amorosi, A., Lo Presti, V., Mastronuzzi, G., Deiana, G., De Falco, G., Fontana, A., Fontolan, G., Lisco, S., Marsico, A., Moretti, M., Orrù, P.E., Sannino, G.M., Serpelloni, E., Vecchio, A., 2017. Sea-level rise and potential drowning of the Italian coastal plains: flooding risk scenarios for 2100. Quat. Sci. Rev. 158, 29–43.

Ariffin, E.H., Mathew, M.J., Roslee, A., Ismailluddin, A., Yun, L.S., Putra, A.B., et al., 2023. A multi-hazards coastal vulnerability index of the east coast of Peninsular Malaysia. Int. J. Disaster Risk Reduc. 84, 103484.

Attri, S.D., Singh, S., Dhar, A., Powar, S., 2022. Multi-attribute sustainability assessment of wastewater treatment technologies using combined fuzzy multi-criteria decision-making techniques. J. Clean. Prod. 357, 131849.

Bajo, M., Međugorac, I., Umgiesser, G., Orlić, M., 2019. Storm surge and seiche modelling in the Adriatic Sea and the impact of data assimilation. Q. J. R. Meteorol. Soc. 145 (722), 2070–2084.

Baldoni, A., Melito, L., Marini, F., Galassi, G., Giacomin, P., Filomena, G., et al., 2024. Modeling coastal inundation for adaptation to climate change at local scale: the case of Marche Region (central Italy). Frontiers in Climate 6, 1334625.

Balica, S.F., Wright, N.G., Van der Meulen, F., 2012. A flood vulnerability index for coastal cities and its use in assessing climate change impacts. Nat. Hazards 64, 73–105.

Barić, A., Grbec, B., Bogner, D., 2008. Potential implications of sea-level rise for Croatia. J. Coast Res. 24 (2), 299–305.

Barzehkar, M., Parnell, K.E., Soomere, T., Dragovich, D., Engström, J., 2021. Decision support tools, systems and indices for sustainable coastal planning and management: a review. Ocean Coast Manag. 212, 105813.

Batista, C.M., 2018. Coastal boundaries. Encyclopedia of Coastal Science 1, 414–426.

Batzakis, D.V., Karymbalis, E., Tsanakas, K., 2024. Assessing coastal vulnerability to climate change-induced hazards in the Eastern Mediterranean: a comparative review of methodological approaches. Geographical Information Science 253–278.

Berman, K., Kuleshov, Y., 2023. Assessing tropical cyclone risk in Australia using community exposure–vulnerability indices. Climate 11 (12), 235.

Bernot, F., 1983. Vzroki in Pogostost Poplav Ob Slovenski Obali. V: Gams, I.(Ur). Naravne nesreče kot naša ogroženost. Ljubljana, SAZU, pp. 50–53.

Bhattachan, A., Emanuel, R.E., Ardon, M., Bernhardt, E.S., Anderson, S.M., Stillwagon, M.G., et al., 2018. Evaluating the effects of land-use change and future climate change on vulnerability of coastal landscapes to saltwater intrusion. Elem Sci Anth 6, 62.

Bilskie, M.V., Hagen, S.C., Medeiros, S.C., Passeri, D.L., 2014. Dynamics of sea level rise and coastal flooding on a changing landscape. Geophys. Res. Lett. 41 (3), 927–934.

Bosello, F., De Cian, E., 2014. Climate change, sea level rise, and coastal disasters. A review of modeling practices. Energy Econ. 46, 593–605.

Brzović, N., Mahović, N.S., 1999. Cyclonic activity and severe jugo in the Adriatic. Phys. Chem. Earth - Part B Hydrol., Oceans Atmos. 24 (6), 653–657.

Bujak, D., Carević, D., Bogovac, T., Kulić, T., 2023. Hindcast of significant wave heights in sheltered basins using machine learning and the Copernicus database. Naše more: znanstveni časopis za more i pomorstvo 70 (2), 103–114.

Burkett, V., Davidson, M., 2012. Coastal Impacts, Adaptation, and Vulnerabilities. Island Press.

Calil, J., Reguero, B.G., Zamora, A.R., Losada, I.J., Méndez, F.J., 2017. Comparative coastal risk index (CCRI): a multidisciplinary risk index for Latin America and the Caribbean. PLoS One 12 (11), e0187011.

Chao, S.R., Ghansah, B., Grant, R.J., 2021. An exploratory model to characterize the vulnerability of coastal buildings to storm surge flooding in Miami-Dade County, Florida. Appl. Geogr. 128, 102413.

Cissé, C.O.T., Marić, I., Domazetović, F., Glavačević, K., Almar, R., 2024. Derivation of coastal erosion susceptibility and socio-economic vulnerability models for sustainable coastal management in Senegal. Sustainability 16, 7422. https://doi.org/10.3390/su16177422, 2024.

Copernicus, 2024. CORINE land cover. https://land.copernicus.eu/en/products/corine-land-cover. (Accessed 29 February 2024).

Copernicus Marine Surface, 2024. https://data.marine.copernicus.eu/product/MEDSEA_MULTIYEAR_WAV_006_012/download. (Accessed 2 March 2024).

Cutter, S.L., 1996. Vulnerability to environmental hazards. Prog. Hum. Geogr. 20 (4), 529–539.

Cutter, S.L., Emrich, C.T., Webb, J.J., Morath, D., 2009. Social vulnerability to climate variability hazards: a review of the literature. Final Report to Oxfam America 5, 1–44.

DEM Over Europe from the GMES RDA Project (EU-DEM, Resolution 25m) - Version 1.

Domazetović, F., Šiljeg, A., Lončar, N., Marić, I., 2019. Development of automated multicriteria GIS analysis of gully erosion susceptibility. Appl. Geogr. 112, 102083.

Domazetović, F., Šiljeg, A., Marić, I., Faričić, J., Vassilakis, E., Panđa, L., 2021. Automated coastline extraction using the very high resolution worldview (WV) satellite imagery and developed coastline extraction tool (CET). Appl. Sci. 11 (20), 9482.

Dorman, C.E., Carniel, S., Cavaleri, L., Sclavo, M., Chiggiato, J., Doyle, J., et al., 2006. February 2003 marine atmospheric conditions and the bora over the northern Adriatic. J. Geophys. Res.: Oceans 111 (C3).

Dow, K., 1992. Exploring differences in our common future (s): the meaning of vulnerability to global environmental change. Geoforum 23 (3), 417–436.

Dukec, D., Kecek, D., Klopotan, I., 2020. Empirical Analysis of tourism impact on Croatian GDP. Economic and Social Development: Book of Proceedings, pp. 389–396.

DZS, 2022. Census of population, households and dwellings in 2021 - population by settlements. https://dzs.gov.hr/vijesti/objavljeni-konacni-rezultati-popisa-2021/1270. (Accessed 31 August 2024).

DZS, 2024. Dolasci i noćenja turista u 2023. godini, TUR-2023-1-2. ISSN 1334-0557, Zagreb 29. veljače, 2024. Godine, available at: https://mint.gov.hr/UserDocsImages/2024_dokumenti/DZS_tur_promet_2023.pdf. (Accessed 31 August 2024).

El-Shahat, S., El-Zafarany, A.M., El Seoud, T.A., Ghoniem, S.A., 2021. Vulnerability assessment of African coasts to sea level rise using GIS and remote sensing. Environ. Dev. Sustain. 23, 2827–2845.

Felsenstein, D., Lichter, M., 2014. Social and economic vulnerability of coastal communities to sea-level rise and extreme flooding. Nat. Hazards 71, 463–491.

Fitra, J., Debataraja, S.M.T., Lismawaty, L., 2024. Identification of flood vulnerability using the topographic wetness index method in Pantai Labu Baru village, Deli Serdang, North Sumatera. In: E3S Web of Conferences, vol. 483. EDP Sciences, p. 1014.

Furlan, E., Dalla Pozza, P., Michetti, M., Torresan, S., Critto, A., Marcomini, A., 2021. Development of a multi-dimensional coastal vulnerability index: assessing vulnerability to inundation scenarios in the Italian coast. Sci. Total Environ. 772, 144650.
Gargiulo, C., Battarra, R., Tremiterra, M.R., 2020. Coastal areas and climate change: a decision support tool for implementing adaptation measures. Land Use Pol. 91, 104413.
GEBCO Gridded Bathymetry Data, available at: https://www.gebco.net/data_and_products/gridded_bathymetry_data/.
Geofabrik. https://www.geofabrik.de/data/download.html. (Accessed 29 February 2024).
Giannakidou, C., Diakoulaki, D., Memos, C.D., 2020. Vulnerability to coastal flooding of industrial urban areas in Greece. Environmental Processes 7, 749–766.
Global Wind Atlas, 2024. https://globalwindatlas.info/en. (Accessed 29 February 2024).
Gornitz, V., 1991. Global coastal hazards from future sea level rise. Palaeogeogr. Palaeoclimatol. Palaeoecol. 89 (4), 379–398.
Gornitz, V.M., White, T.W., Daniels, R.C., 1997. In: A Coastal Hazards Data Base for the US West Coast (1997)(NDP-043C). Environmental System Science Data Infrastructure for a Virtual Ecosystem (ESS-DIVE)(United States). https://doi.org/10.3334/CDIAC/ssr.ndp043c. No. osti: 1389517; doi: 10.3334/CDIAC/SSR. NDP043C; cdiac.
Griggs, G., Reguero, B.G., 2021. Coastal adaptation to climate change and sea-level rise. Water 13 (16), 2151.
Hawchar, L., Naughton, O., Nolan, P., Stewart, M.G., Ryan, P.C., 2020. A GIS-based framework for high-level climate change risk assessment of critical infrastructure. Climate Risk Management 29, 100235.
HHI, 2024. Hydrographic institute of the republic of Croatia. Adriatic Sea Level available at: https://www.hhi.hr/en/about-us/projects/adriatic-sea-level#:~:text=Mean/20daily/20tidal/20range/20along,and/2047/20cm/20at/20Rovinj. (Accessed 31 August 2024).
Horton, B.P., Khan, N.S., Cahill, N., Lee, J.S., Shaw, T.A., Garner, A.J., et al., 2020. Estimating global mean sea-level rise and its uncertainties by 2100 and 2300 from an expert survey. NPJ climate and atmospheric science 3 (1), 18.
Hrvatske vode, 2024. Registar poplavnih događaja. https://voda.hr/hr/registar-poplavnih-dogadaja.
Idier, D., Bertin, X., Thompson, P., Pickering, M.D., 2019. Interactions between mean sea level, tide, surge, waves and flooding: mechanisms and contributions to sea level variations at the coast. Surv. Geophys. 40 (6), 1603–1630.
Ietto, F., Cantasano, N., Pellicone, G., 2018. A new coastal erosion risk assessment indicator: application to the Calabria Tyrrhenian Littoral (southern Italy). Environmental Processes 5, 201–223.
IPCC, 2019. Summary for policymakers. In: Shukla, P.R., Skea, J., Calvo Buendia, E., Masson-Delmotte, V., Pörtner, H.-O., Roberts, D.C., Zhai, P., Slade, R., Connors, S., van Diemen, R., Ferrat, M., Haughey, E., Luz, S., Neogi, S., Pathak, M., Petzold, J., Portugal Pereira, J., Vyas, P., Huntley, E., Kissick, K., Belkacemi, M., Malley, J. (Eds.), Climate Change and Land: an IPCC Special Report on Climate Change, Desertification, Land Degradation, Sustainable Land Management, Food Security, and Greenhouse Gas Fluxes in Terrestrial Ecosystems.
IPCC, 2023. Summary for policymakers. In: Lee, H., Romero, J. (Eds.), Climate Change 2023: Synthesis Report. Contribution of Working Groups I, II and III to the Sixth Assessment Report of the Intergovernmental Panel on Climate Change [Core Writing Team. IPCC, Geneva, Switzerland, pp. 1–34. https://doi.org/10.59327/IPCC/AR6-9789291691647.001.
Ivandić, N., Šutalo, I., 2018. The contribution of tourism to the Croatian economy: an IO approach. Ekon. Pregl. 69 (1), 20–42.
Johnston, A., Slovinsky, P., Yates, K.L., 2014. Assessing the vulnerability of coastal infrastructure to sea level rise using multi-criteria analysis in Scarborough, Maine (USA). Ocean Coast Manag. 95, 176–188.
Karymbalis, E., Chalkias, C., Chalkias, G., Grigoropoulou, E., Manthos, G., Ferentinou, M., 2012. Assessment of the sensitivity of the southern coast of the Gulf of Corinth (Peloponnese, Greece) to sea-level rise. Cent. Eur. J. Geosci. 4, 561–577.
Karymbalis, E., Chalkias, C., Ferentinou, M., Chalkias, G., Magklara, M., 2014. Assessment of the sensitivity of salamina (saronic Gulf) and elafonissos (lakonic Gulf) islands to sea-level rise. J. Coast Res. (70), 378–384.
Katalinić, M., Parunov, J., 2018. Wave statistics in the Adriatic Sea based on 24 years of satellite measurements. Ocean Eng. 158, 378–388.
Katalinić, M., Ćorak, M., Parunov, J., 2014. Analysis of wave heights and wind speeds in the Adriatic Sea. Maritime Technology and Engineering 1, 1389–1394.
Kelletat, D.H., 2019. Dalmatian coasts. In: Finkl, C.W., Makowski, C. (Eds.), Encyclopedia of Coastal Science. Encyclopedia of Earth Sciences Series. Springer, Cham.
Koboević, Ž., Milošević-Pujo, B., Kurtela, Ž., 2012. Održivi razvoj i integrirano upravljanje obalnim područjem–procesi uspješne zaštite obalnog mora. NAŠE MORE: znanstveni časopis za more i pomorstvo 59 (3–4), 176–188.
Kolega, N., 2006. Slovenian coast sea floods risk. Acta Geogr. Slov. 46 (2), 143–167.
Kraus, R., Grilli, F., Supić, N., Janeković, I., Brailo, M., Cara, M., et al., 2019. Oceanographic characteristics of the Adriatic Sea–Support to secondary HAOP spread through natural dispersal. Mar. Pollut. Bull. 147, 59–85.
Kumar, T.S., Mahendra, R.S., Nayak, S., Radhakrishnan, K., Sahu, K.C., 2010. Coastal vulnerability assessment for Orissa State, east coast of India. J. Coast Res. 26 (3), 523–534.
Lipizer, M., Partescano, E., Rabitti, A., Giorgetti, A., Crise, A., 2014. Qualified temperature, salinity and dissolved oxygen climatologies in a changing Adriatic Sea. Ocean Sci. 10 (5), 771–797.
Liu, J., Wen, J., Huang, Y., Shi, M., Meng, Q., Ding, J., Xu, H., 2015. Human settlement and regional development in the context of climate change: a spatial analysis of low elevation coastal zones in China. Mitig. Adapt. Strategies Glob. Change 20, 527–546.
Loizidou, X.I., Orthodoxou D I, L., Loizides, M., Petsa, D., Anzidei, M., 2024. Adapting to sea level rise: participatory, solution-oriented policy tools in vulnerable Mediterranean areas. Environment Systems and Decisions 44 (1), 126–144.
Lozano, C.J., Candela, J., 1995. The M (2) tide in the Mediterranean Sea: dynamic analysis and data assimilation. Oceanol. Acta 18 (4), 419–441.
Magaš, D., 2013. Geografija Hrvatske. Meridijani, Zagreb, Hrvatska.
Mahapatra, M., Ramakrishnan, R., Rajawat, A.S., 2015. Coastal vulnerability assessment using analytical hierarchical process for South Gujarat coast, India. Nat. Hazards 76, 139–159.
Mani Murali, R., Ankita, M., Amrita, S., Vethamony, P., 2013. Coastal vulnerability assessment of Puducherry coast, India, using the analytical hierarchical process. Nat. Hazards Earth Syst. Sci. 13 (12), 3291–3311.
Marić, I., Šiljeg, A., Domazetović, F., 2021. Derivation of wildfire ignition index using GIS-MCDA from high-resolution UAV imagery data and perception analysis in settlement sali, dugi otok island (Croatia). In: Proceedings of the 7th International Conference on Geographical Information Systems Theory, Applications and Management (GISTAM 2021), pp. 90–97.
Mavromatidi, A., Briche, E., Claeys, C., 2018. Mapping and analyzing socio-environmental vulnerability to coastal hazards induced by climate change: an application to coastal Mediterranean cities in France. Cities 72, 189–200.
McGranahan, G., Balk, D., Anderson, B., 2007. The rising tide: assessing the risks of climate change and human settlements in low elevation coastal zones. Environ. Urbanization 19 (1), 17–37.
Mclaughlin, S., Cooper, J.A.G., 2010. A multi-scale coastal vulnerability index: a tool for coastal managers? Environ. Hazards 9 (3), 233–248.
Međugorac, I., Pasarić, M., Orlić, M., 2015. Severe flooding along the eastern Adriatic coast: the case of 1 December 2008. Ocean Dynam. 65, 817–830.
Međugorac, I., Orlić, M., Janeković, I., Pasarić, Z., Pasarić, M., 2018. Adriatic storm surges and related cross-basin sea-level slope. J. Mar. Syst. 181, 79–90.
Medvedev, I.P., Vilibić, I., Rabinovich, A.B., 2020. Tidal resonance in the Adriatic Sea: observational evidence. J. Geophys. Res.: Oceans 125 (8), e2020JC016168.
Mićunović, M., Faivre, S., 2023. Toward the vulnerability assessment of the island of Hvar beaches Croatia, Central Adriatic. In: 8. *Hrvatski Geografski Kongres-Geografski Odgovori Na Izazove Suvremenog Svijeta U 21. Stoljeću I 140 Godina Geografije Na Sveučilištu U Zagrebu*, pp. 233–234.
Ministry of the Sea, Transport and Infrastructure, 2011. Otoci i priobalje. https://mmpi.gov.hr/more/otoci-i-priobalje/8322. (Accessed 30 August 2024).
Mohamed, S.A., 2020. Coastal vulnerability assessment using GIS-Based multicriteria analysis of Alexandria-northwestern Nile Delta, Egypt. J. Afr. Earth Sci. 163, 103751.
Muler, M., Bonetti, J., 2014. An integrated approach to assess wave exposure in coastal areas for vulnerability analysis. Mar. Geodesy 37 (2), 220–237.
Ng, K., Borges, P., Phillips, M.R., Medeiros, A., Calado, H., 2019. An integrated coastal vulnerability approach to small islands: the Azores case. Sci. Total Environ. 690, 1218–1227.
Osorio-Cano, J.D., Alcérreca-Huerta, J.C., Mariño-Tapia, I., Osorio, A.F., Acevedo-Ramírez, C., Enriquez, C., et al., 2019. Effects of roughness loss on reef hydrodynamics and coastal protection: approaches in Latin America. Estuar. Coast 42, 1742–1760.
Palmer, B.J., Van der Elst, R., Mackay, F., Mather, A.A., Smith, A.M., Bundy, S.C., et al., 2011. Preliminary coastal vulnerability assessment for kwazulu-natal, South Africa. J. Coast Res. 1390–1395.
Pantusa, D., D'Alessandro, F., Riefolo, L., Principato, F., Tomasicchio, G.R., 2018. Application of a coastal vulnerability index. A case study along the Apulian Coastline, Italy. Water 10 (9), 1218.
Parthasarathy, A., Natesan, U., 2015. Coastal vulnerability assessment: a case study on erosion and coastal change along Tuticorin, Gulf of Mannar. Nat. Hazards 75, 1713–1729.
Portman, M.E., Esteves, L.S., Le, X.Q., Khan, A.Z., 2012. Improving integration for integrated coastal zone management: an eight country study. Sci. Total Environ. 439, 194–201.
Pramanik, M.K., Biswas, S.S., Mondal, B., Pal, R., 2016. Coastal vulnerability assessment of the predicted sea level rise in the coastal zone of Krishna–Godavari delta region, Andhra Pradesh, east coast of India. Environ. Dev. Sustain. 18, 1635–1655.
Queffeulou, P., Bentamy, A., 2007. Analysis of wave height variability using altimeter measurements: application to the Mediterranean Sea. J. Atmos. Ocean. Technol. 24 (12), 2078–2092.
Rabby, Y.W., Hossain, M.B., Hasan, M.U., 2019. Social vulnerability in the coastal region of Bangladesh: an investigation of social vulnerability index and scalar change effects. Int. J. Disaster Risk Reduc. 41, 101329.
Ramnalis, P., Batzakis, D.V., Karymbalis, E., 2023. Applying two methodologies of an integrated coastal vulnerability index (ICVI) to future sea-level rise. Case study: southern coast of the Gulf of Corinth, Greece. Geoadria 28 (1), 1–24.
Ribas, A., Olcina, J., Sauri, D., 2020. More exposed but also more vulnerable? Climate change, high intensity precipitation events and flooding in Mediterranean Spain. Disaster Prev. Manag. 29 (3), 229–248.
Rossi, I.R., Karavanić, I., Butorac, V., 2020. Croatia: submerged prehistoric sites in a karstic landscape. The Archaeology of Europe's Drowned Landscapes, pp. 347–369.
Roukounis, C.N., Tsihrintzis, V.A., 2022. Indices of coastal vulnerability to climate change: a review. Environmental Processes 9 (2), 29.
Ružić, I., Dugonjić Jovančević, S., Benac, Č., Krvavica, N., 2019. Assessment of the coastal vulnerability index in an area of complex geological conditions on the Krk Island, Northeast Adriatic Sea. Geosciences 9 (5), 219.

Satta, A., 2014. An Index-Based Method to Assess Vulnerabilities and Risks of Mediterranean Coastal Zones to Multiple Hazards. Department of Economics, Ca' Foscari University of, Venice, Italy. PhD Dissertation.
Satta, A., Snoussi, M., Puddu, M., Flayou, L., Hout, R., 2016. An index-based method to assess risks of climate-related hazards in coastal zones: the case of Tetouan. Estuarine. Coastal and Shelf Science 175, 93–105.
Šiljeg, A., Marić, I., Cukrov, N., Domazetović, F., Roland, V., 2020. A multiscale framework for sustainable management of tufa-forming watercourses: a case study of National Park "Krka". Croatia. Water 12 (11), 3096.
Šimac, Z., Lončar, N., Faivre, S., 2023. Overview of coastal vulnerability indices with reference to physical characteristics of the Croatian Coast of Istria. Hydrology 10 (1), 14.
Sokolić, J., 1994. Otok susak-mogućnosti revitalizacije. Društvena Istraživanja: časopis za opća društvena pitanja 3 (4–5), 503–515, 12-13.
Stanley, D.J., 1995. A global sea-level curve for the late Quaternary: the impossible dream? Mar. Geol. 125 (1–2), 1–6.
Szlafsztein, C., Sterr, H., 2007. A GIS-based vulnerability assessment of coastal natural hazards, state of Pará, Brazil. J. Coast Conserv. 11, 53–66.
Tano, R.A., Aman, A., Kouadio, K.Y., Toualy, E., Ali, K.E., Assamoi, P., 2016. Assessment of the Ivorian coastal vulnerability. J. Coast Res. 32 (6), 1495–1503.
Thiébault, S., Moatti, J.P., 2016. The Mediterranean Region under Climate Change: a Scientific Update. IRD Éditions/AllEnvi, Marseille.
Tibbetts, J.R., van Proosdij, D., 2013. Development of a relative coastal vulnerability index in a macro-tidal environment for climate change adaptation. J. Coast Conserv. 17, 775–797.
Topography Tools for ArcGIS 10.3. https://hub.arcgis.com/content/b13b3b40fa3c43d4a23a1a09c5fe96b9/about. (Accessed 29 February 2024).
Torresan, S., Critto, A., Rizzi, J., Marcomini, A., 2012. Assessment of coastal vulnerability to climate change hazards at the regional scale: the case study of the North Adriatic Sea. Nat. Hazards Earth Syst. Sci. 12 (7), 2347–2368.
Toubes, D.R., Gössling, S., Hall, C.M., Scott, D., 2017. Vulnerability of coastal beach tourism to flooding: a case study of Galicia, Spain. Environments 4 (4), 83.
Tragaki, A., Gallousi, C., Karymbalis, E., 2018. Coastal hazard vulnerability assessment based on geomorphic, oceanographic and demographic parameters: the case of the Peloponnese (Southern Greece). Land 7 (2), 56.
United Nations International Strategy for Disaster Reduction (UN/ISDR), 2004. Living with Risk. A Global Review of Disaster Reduction Initiatives. UN Publications, Geneva. https://www.unisdr.org/files/7817_7819isdrterminology11.pdf.
UPRIMO, 2022. Studija upravljanja rizicima od poplava mora (VEPAR), Zagreb, Septembe 9, 2024. https://voda.hr/sites/default/files/dokumenti/PUVP3/20-/20URP/20-/200011.pdf.
URL1. https://www.eurostarumag.hr/istra/kaos-duz-obale-a-strucnjaci-kazu-nezapamceno-da-jugo-traje-ovako-dugo-bit-ce-i-gore/. (Accessed 6 May 2024).
URL10. https://www.057info.hr/vijesti/2024-03-11/nad-zadrom-se-nocas-ispraznio-oblak-sa-164-litra-kise-po-metru-cetvornom-jugo-je-poplavilo-rivu/. (Accessed 7 May 2024).
URL11. https://www.jutarnji.hr/vijesti/hrvatska/foto-olujno-jugo-na-rabu-poplavilo-rivu-2226443. (Accessed 7 May 2024).
URL12. https://www.tportal.hr/vijesti/clanak/snazno-jugo-poplavilo-trznicu-u-rijeci-postavljaju-se-vrece-s-pijeskom-foto-20231027?meta_refresh=1. (Accessed 7 May 2024).
URL13. https://www.morski.hr/rive-i-ceste-posvuda-pod-morem-vela-luka-hvar-split-trogir-sibenik-pag-rovinj/. (Accessed 7 May 2024).
URL14. https://www.novilist.hr/rijeka-regija/novi-vinodolski-crikvenica/nevrijeme-u-senju-poplavile-zgrade-odroni-na-cestama-osteceni-automobili-i-plovila/. (Accessed 23 May 2024).
URL2. https://www.otoci.net/index.php/u-razno/16674-cres-jedno-od-ugrozenijih-naselja-u-regiji. (Accessed 6 May 2024).
URL3. https://www.istriaterramagica.eu/novosti/zatvoren-antenal-za-promet/. (Accessed 6 May 2024).
URL4. https://dalmatinskiportal.hr/vijesti/foto-video-jugo-poplavilo-kastelansku-rivu/184301. (Accessed 6 May 2024).
URL5. https://www.vecernji.hr/vijesti/olujno-jugo-poplavilo-rivu-u-vodicama-nevrijeme-zahvatilo-dalmaciju-911976. (Accessed 6 May 2024).
URL6. https://slobodnadalmacija.hr/split/splitska-riva-poplavila-pod-naletima-olujnog-juga-pogledajte-impresivne-kadrove-naseg-fotoreportera-1335786. (Accessed 6 May 2024).
URL7. https://www.novilist.hr/rijeka-regija/otoci/jako-jugo-i-kisa-more-poplavilo-cresku-rivu/. (Accessed 6 May 2024).
URL8. https://net.hr/danas/vijesti/jako-jugo-izazvalo-kaos-u-dalmaciji-valovi-zapljuskali-rivu-u-vodicama-i-otezavali-promet-133754c4-b9ef-11ec-982b-0242ac120057. (Accessed 6 May 2024).
URL9. https://sibenskiportal.hr/zupanija/vodice/foto-olujno-jugo-poplavilo-vodicku-rivu/. (Accessed 6 May 2024).
Viličić, D., 2014. Specific oceanological characteristics of the Croatian part of the Adriatic. Hrvat. Vode 22 (90), 297–314.
Vitousek, S., Barnard, P.L., Fletcher, C.H., Frazer, N., Erikson, L., Storlazzi, C.D., 2017. Doubling of coastal flooding frequency within decades due to sea-level rise. Sci. Rep. 7 (1), 1399.
Vujičić, J., 2024. Analiza Plavljenja Hrvatskih Obalnih Naselja. Department of Geography, University of Zadar, Zadar, Croatia. Master Thesis.
Wahl, T., Jain, S., Bender, J., Meyers, S.D., Luther, M.E., 2015. Increasing risk of compound flooding from storm surge and rainfall for major US cities. Nat. Clim. Change 5 (12), 1093–1097.
Yahia Meddah, R., Ghodbani, T., Senouci, R., Rabehi, W., Duarte, L., Teodoro, A.C., 2023. Estimation of the coastal vulnerability index using multi-criteria decision making: the coastal social–ecological system of rachgoun, western Algeria. Sustainability 15 (17), 12838.
Zampazas, G., Karymbalis, E., Chalkias, C., 2022. Assessment of the sensitivity of zakynthos island (Ionian Sea, western Greece) to climate change-induced coastal hazards. Zeitschrift Fur Geomorphol 63 (2–3), 183–200.
Zanetti, V.B., de Sousa Jr., W.C., de Freitas, D.M., 2016. A climate change vulnerability index and case study in a Brazilian Coastal City. Sustainability 8 (8), 1–12.
Zhang, Y., Wu, T., Arkema, K.K., Han, B., Lu, F., Ruckelshaus, M., Ouyang, Z., 2021. Coastal vulnerability to climate change in China's Bohai Economic Rim. Environ. Int. 147, 106359.